UNIVERSITY of CALIFORNIA
SANTA CRUZ

FIR EXCESS IN RED SEQUENCE GALAXIES

A thesis submitted in partial satisfaction of the
requirements for the degree of

BACHELOR OF SCIENCE

in

PHYSICS

by

Heather Busk

11 March 2010

The thesis of Heather Busk is approved by:

Professor David Koo
Advisor

Professor David P. Belanger
Senior Theses Coordinator

Professor David P. Belanger
Chair, Department of Physics

Abstract

FIR Excess in Red Sequence Galaxies

by

Heather Busk

The red sequence is generally regarded as made up of galaxies that have stopped forming stars at any significant level. Certain galaxies have been found that do not have any emission lines suggestive of star formation or an active galactic nucleus, yet have a far infrared emission that is a factor of 10 or more higher than is expected from a population of old stars. To examine the cause of this, red sequence galaxies without emission lines were divided into two groups, of detected objects having non-zero 24μm emission (the objects with FIR excess), and non-detected objects with no recorded 24μm emission. Color-magnitude diagrams comparing objects with and without 24μm emission show that galaxies with an excess tend to be bluer and brighter than the general red sequence. Hubble Space Telescope color images of a portion of the detected galaxies were compared to non-detected objects at similar redshifts. Of the detected objects, 10 had clumps of blue within half a radius of the object, compared to 2 of the non-detected. All but three of the detected objects were larger than the non-detected objects at a comparable redshift, and only one was smaller than the comparison object. The set of model SEDs (Spectral Energy Distributions) created by Maraston were fitted to the SED for each object, producing an estimate of the ages and τ's (rate of decay of the star formation rate). The ages tend to be slightly larger and the τ's tend to be slightly longer for the detected objects than for the non-detected, though this trend remains to be confirmed and interpreted. These results suggest the excess may be caused by ongoing star formation, despite the lack of emission lines. This project used optical and infrared data from the AEGIS collaboration, and spectroscopic data from the DEEP2 redshift survey.

List of Figures

List of Tables

Acknowledgements

I would like to thank David Rosario, for his advice and patience. More materially, he provided IDL programs to quickly display spectra, SEDs, and multiwavelength images, and a program to fit the set of Maraston models to the SEDs. I'd also like to thank David Koo for his help, especially his advice on the importance of planning. This study makes use of data from AEGIS, a multiwavelength sky survey conducted with the Chandra, GALEX, Hubble, Keck, CFHT, MMT, Subaru, Palomar, Spitzer, VLA, and other telescopes and supported in part by the NSF, NASA, and the STFC.

1 Introduction

It has recently been demonstrated that galaxies fall roughly into two groups.[1] One group, called the red sequence (RS), is redder and brighter, while the other group, called the Blue Cloud, is bluer and dimmer. There are fewer galaxies with an intermediate color. This echoes the traditional morphological division of galaxy types into blue spirals and red ellipticals, but adds a connection to luminosity.

The bimodality of galaxies is an important clue about the evolution of galaxies through time. To understand why, it is necessary to explore the meaning of a galaxy's color. A galaxy's light is a superposition of the light from all of its stars, gas, and dust. A star emits with roughly a blackbody spectrum, with a peak emission wavelength depending on its temperature, such that hotter stars emit at shorter wavelengths. Massive young stars are hot, and emit most strongly in the ultraviolet (UV). When observed through optical filters they appear blue. Thus, if a galaxy has ongoing or recent star formation, it will appear blue. Old stars, in contrast, appear red, and in the absence of significant star formation in the galaxy, the light from these stars will dominate, making the galaxy red.

The consequences of this are that the red sequence is populated by galaxies with an older stellar population and the blue cloud is populated by galaxies forming stars. However, dust (solid particles floating in space roughly a micron to a millimeter in size that are composed of a variety of elements) also causes reddenning, by preferentially scattering blue light. Thus, blue light from a galaxy will be attenuated, while not much affecting the red light.[2] A very dusty galaxy can be present on the red sequence, despite being intrinsically blue.[3]

Infrared (IR) light is useful as a tracer of dust, because dust reprocesses UV radiation into IR. Infrared light has wavelengths from about 1μm to 300μm. The near-IR (NIR) covers the wavelength range from roughly 1μm to 2μm, the mid-IR (MIR) stretches from 2.4μm to 20μm, and the FIR has wavelengths greater than about 20μm.[2] Massive young stars have a peak emission in the UV. However, stars form in clouds filled with dust, and dust blocks much of the UV light and reemits it in the FIR. Similarly, Active Galactic Nuclei

(AGN) produce MIR radiation. An AGN is formed as a disk of gas and dust is accreted onto an SMBH (Supermassive Black Hole) at the center of the galaxy. The disk heats up and emits copious amounts of high energy radiation, which is reemited in the IR by dust. Emission lines can indicate whether star formation or AGN are present. The UV produced by young stars and AGN ionize the surrounding gas.[2,4] As some of the electrons that were ejected recombine with the atoms, they emit photons whose combined energy corresponds to the ionization energy.

A portion of red sequence galaxies have emission lines from star formation or AGN, and as expected, an elevated level of IR emission. However, some red sequence objects produce more infrared light than expected for a stellar population composed of only old stars, yet lack emission lines. This project has explored the cause of FIR excess in such objects.

There are a number of possible ways to produce an FIR excess without obvious signs of star formation or an AGN. All of them require heating of dust by some source of energy. If forming stars or an AGN are heavily enshrouded by dust, the emission lines can be blocked by the dust. Such thick dust may be visible in an optical image as dust clouds, if they are large enough. This makes high quality images valuable. Low levels of star formation can produce lines that are not strong enough to be detected. Dust distributed diffusely throughout the galaxy could be heated by old stars or possibly radiation from a now faded AGN.[5] No significant production of emission lines will occur without adequate gas near the sources of ionizing radiation, since the radiation intensity falls off with distance.

In Section 2, I will discuss the selection of the sample. This includes precisely defining the red sequence, examining galaxy spectra for the presence of emission lines, and doublechecking that objects identified at 24μm are the same objects identified in other wavelengths. In Section 3, I discuss the tools used to dissect the sample. ACS color images were examined for the presence of visible dust, young blue stars, and unusual morphology. A model spectral energy distribution (SED) was fit to the photometry of each object to measure the amount of FIR excess (at 24μm), calculate star formation histories and ages of the galaxies, and in general to characterize the photometry of the objects. CMDs of objects with and without

24μm emission in various distance bins were plotted to uncover any disparities between these two populations. In Section 4, I discuss the results. In Section 5, I summarize this work and remark on further work to be done.

2 Sample Selection

2.1 Definitions

A few definitions will prove useful.

B-band absolute magnitude (M_B) is a measure of the luminosity of an object in the B-band (B for blue, at a wavelength of around 445nm), adjusted for the dimming caused by large distance. Magnitude is given by

$$m = -2.5log(F/F_{vega}) + m_{vega}, \tag{1}$$

$$M = m - 5log(\frac{D}{1pc}) + 5 \tag{2}$$

where F is the flux (energy emitted per second per unit area) of the object in the B-band, F_{vega} is the flux of the reference star Vega in the B-band, m and M are the apparent and absolute magnitudes, and D is the luminosity distance to the object.

The concept of color can be extended beyond the color visible with the eye to non-optical wavelengths. U-B color is determined by subtracting the object's magnitude in the B-band from its magnitude in the U-band (U for ultraviolet, near a wavelength of 365nm). Color gives the object's relative brightness in two different regions of the spectrum. Red objects will be brighter in the red part of the spectrum than in the blue part.

Redshift (z) is given by

$$z = \frac{\lambda_{obs} - \lambda_{em}}{\lambda_{em}}, \tag{3}$$

where λ_{obs} and λ_{em} are the observed and emitted wavelengths of a known emission or absorption line. λ_{em} is the wavelength of light that would be observed in the galaxy's rest

frame, or the reference frame where the galaxy would appear to be at rest. The universe is expanding, so light is redshifted (its wavelength increased) as the space it travels through stretches. This shifts the original λ_{em} to λ_{obs} by the time it arrives at earth. Together with some assumptions about the past expansion of the universe, redshift can be used to determine the distance to an object, and thus its true magnitude.

Metallicity is defined as

$$Z = log([Z/H]) \tag{4}$$

where [Z/H] is the ratio of the concentrations of elements heavier than helium to the concentration of hydrogen.[2] Stars produce most of their metals through the process of fusion once they have exhausted their supply of hydrogen, and supernovae produce metals as well. Because of this, as a stellar population ages and stars die, the metallicity increases. High metallicity also causes reddening by increasing the opacity of stellar atmospheres. The metal atoms have a series of UV and blue light absorption lines, and the light blocked by these lines is instead emitted at longer wavelengths.

The objects for this work were taken from the DEEP2 survey. DEEP2 was a systematic spectroscopic survey of over 60,000 galaxies in four regions of the sky.[6,7] It used the DEIMOS spectrograph on the Keck 10-m Telescope. Field 1 (known as the Extended Groth Strip, the EGS) was used in this project. Redshifts for about 10,000 galaxies were measured, and rest frame colors and magnitudes were calculated from these spectra. The photometry for the objects was taken from a catalog created by AEGIS (All-wavelength Extended Groth strip International Survey), a collaboration between several groups, including the DEEP group at UCSC, to examine the EGS in a broad range of wavelengths, from x-ray to radio, as a way to put together a complete picture of the observed objects.[8] The photometry used for this project was made up of data from the CFHT (Canada France Hawaii Telescope-optical), the Palomar 5-m Telescope (NIR), Akari, the Subaru SuprimeCam, the MMT Megacam, the IRAC detector on the Spitzer Space Telescope (MIR), and the MIPS detector (FIR), also on Spitzer. The DEEP catalog provided redshifts and magnitudes for the objects. The EGS

Table 1: Parameters defining the red sequence. The slope is the slope of the lines paralleling the red sequence. The y-intercept is where the line passing through the RS intersects the y-axis. The width is half the vertical distance between the top and bottom lines of the parallelogram. Brightest and faintest magnitudes are the left and right cutoffs, respectively.

redshift range	slope	y-intercept	width	brightest magnitude	faintest magnitude
$0.2 \leq z < 0.4$	-0.06	0.01	0.185	-21.25	-16.75
$0.4 \leq z < 0.6$	-0.047	0.341	0.175	-21.5	-18.4
$0.6 \leq z < 0.8$	-0.05	0.275	0.175	-21.75	-18.75
$0.8 \leq z \leq 1.0$	-0.0333	0.608	0.15	-21.8	-19.8

multiwavelength catalog provided further photometric data for a subset of these objects.

2.2 Defining the red sequence

The first step in selecting the sample of red sequence galaxies without emission lines is defining which objects are on the red sequence. A more precise definition of the red and blue sequences is best illustrated using a standard tool of astronomy, the color-magnitude diagram (CMD). A CMD of galaxies taken from the DEEP2 spectroscopic survey is presented in Fig. 1. The x-axis is the absolute magnitude, and the y-axis is the U-B color. On the diagram, the galaxies clearly fall into two clumps of higher density separated by a region of lower density. The upper clump is the red sequence, the lower clump is the blue sequence, and the area betweem them is called the green valley. There is a definite relationship between the color and the magnitude of objects on the red sequence, such that brighter galaxies are redder. There is some scatter in the CM relation of the red sequence, but it is necessary to make a precise division of red sequence and green valley objects. Drawing a box around the red sequence was sufficient to ensure that only RS galaxies were included. The slope and y-intercept of a line drawn by hand along the red sequence was calculated (presented in Table 1).

Every object within a certain distance of this line and within a range of magnitudes, as chosen by eye, was included in the red sequence. Figure 2 shows CMDs for galaxies in

Figure 1: Color-Magnitude Diagram of DEEP2 objects. Red and bright objects will be to the upper left. The dot color corresponds to redshift range. Purple denotes 0.2≤ z <0.4, red denotes 0.4≤z<0.6, green denotes 0.6≤z<0.8, and black denotes 0.8≤z<1.0.

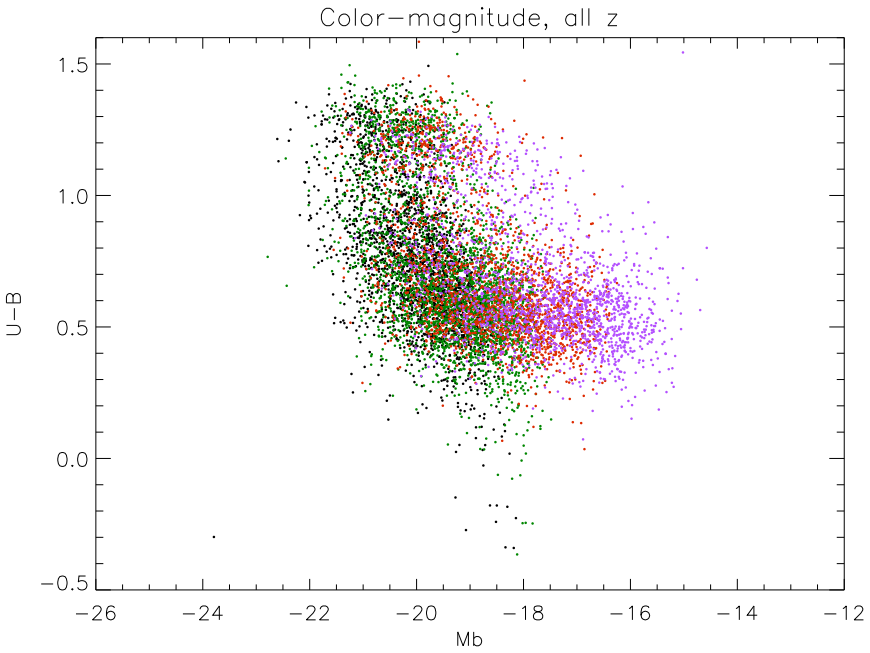

each redshift range, along with the parallelograms defining the red sequence. Their redshifts are all between 0.2 and 1.0 (corresponding to distances of 8.6x10^5 Mpc to 4.3x10^6 Mpc[9]; for comparison, the distance to the Andromeda galaxy is about 0.7 Mpc[10]) and of good quality. The red sequence was defined separately for each redshift range, because its slope and color changes with redshift, as the stars evolve. The width was chosen so that only red sequence galaxies were included, while any outliers and green valley galaxies were excluded. The faintest magnitudes were set to exclude objects at the faint absolute magnitude edge of the sequence. Fainter than this magnitude, the data was incomplete (not all of the galaxies present were recorded), as suggested by the lower density of objects in this area of the diagram. Including this region would not produce legitimate statistics. The blue sequence is less effected by incompleteness, because the survey is sensitive to the rest-frame blue light of these galaxies. Thus, dim blue galaxies were more easily detected than red galaxies of a similar magnitude. The truncation at faint magnitudes is especially evident at redshifts higher than 0.6, so that even the blue sequence is cut off. Higher redshift objects appear dim because of the distance, and if the object is not intrinsically bright enough it will not easily be observed. After this stage of the selection, of the 9253 objects in the DEEP catalog with high quality redshifts, 1267 were on the red sequence.

2.3 Galaxy Spectra

The next step was to examine the spectra of the galaxies in the sample for the presence of emission lines, as a way to root out objects with star formation or an AGN. Many galaxies display emission lines, which can be used to infer a great deal of information about the galaxies. The emission lines listed in Table 2 are lines that indicate star formation and AGN.

After a hydrogen atom is ionized, the free electron will eventually recombine with another atom, and may occupy any of the energy shells. It often initially occupies the n=3 shell, and quickly drops down to a lower shell.[11] Hα corresponds to an electron transition from the n=3 to n=2 shell, and Hβ corresponds to an electron transition from the n=4 to n=2 shell.

Figure 2: CMD used to define the red sequence, in several redshift bins.

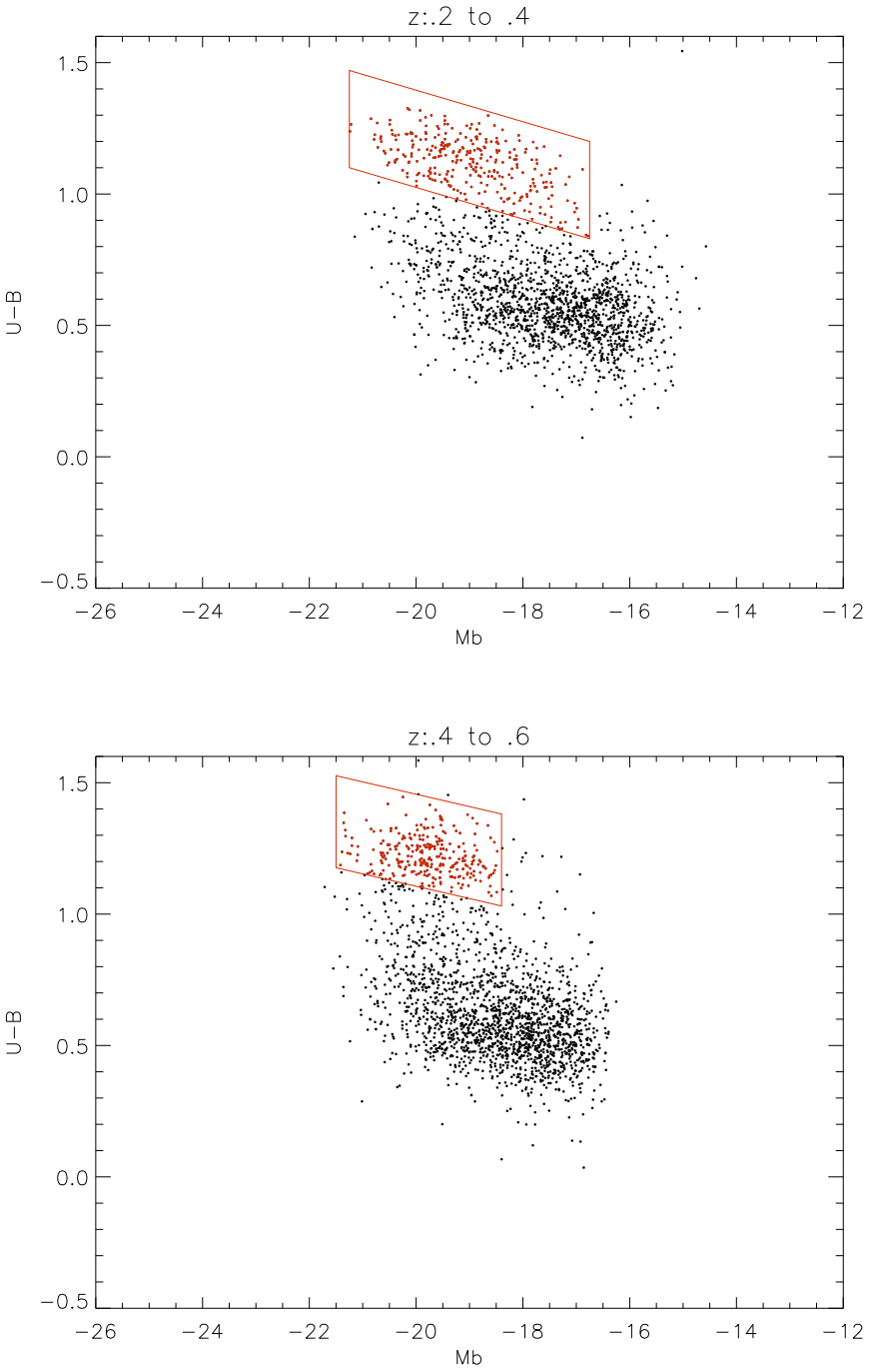

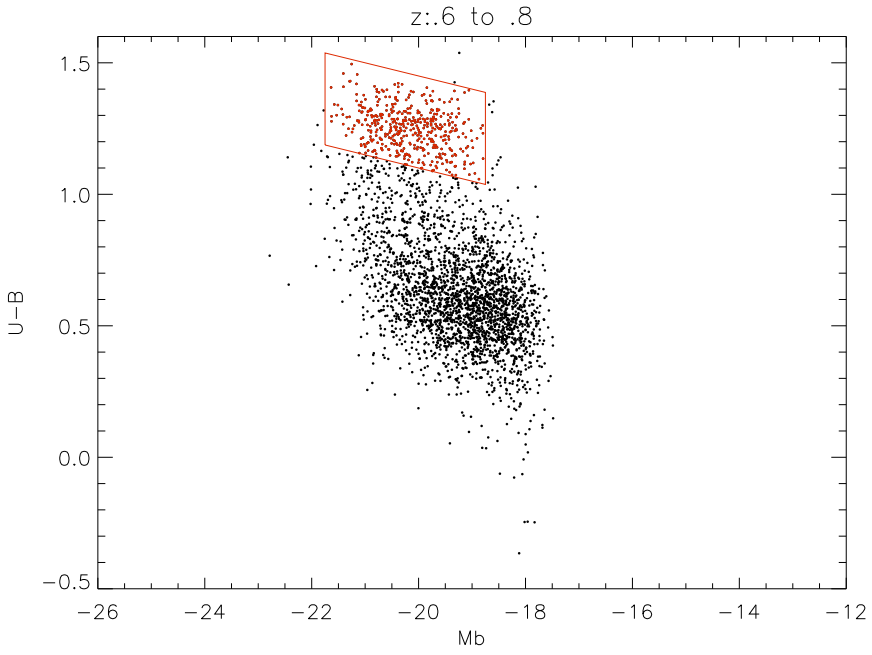
z:.6 to .8
1.5
1.0
0.5
0.0
−0.5
U−B
−26
−24
−22
−20
−18
−16
−14
−12
Mb

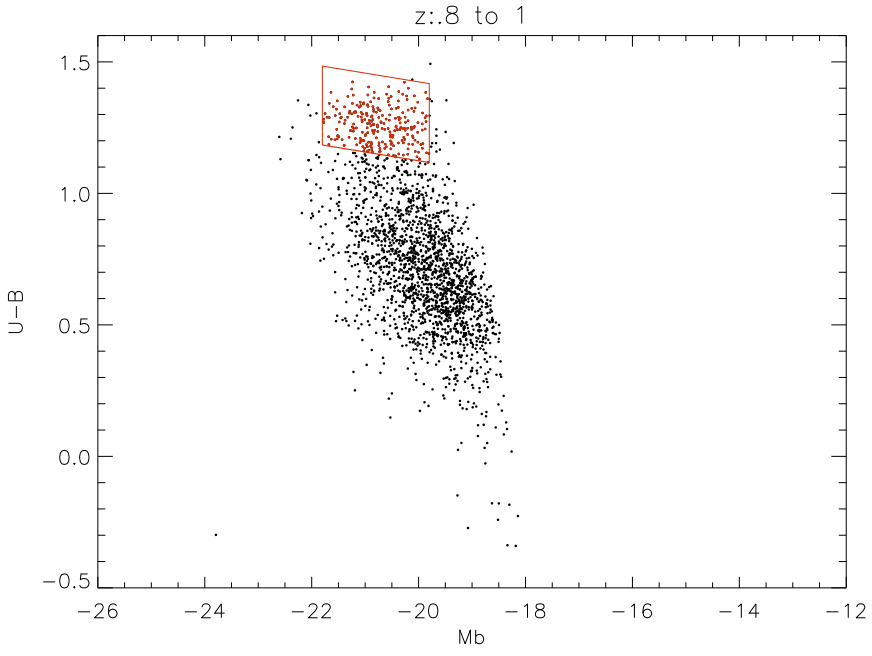
z:.8 to 1
1.5
1.0
0.5
0.0
−0.5
U−B
−26
−24
−22
−20
−18
−16
−14
−12
Mb

Table 2: Emission lines associated with star formation and AGN.

Line	Wavelength (Å)
[OIIa]	3726
[OIIb]	3729
[OIIIa]	4959
[OIIIb]	5007
Hα	6563
Hβ	4861
Hγ	4342
[NII]	6583

Figure 3: 2-D spectrum of Object 12008948.

Since the Hα transition is more likely, Hα will be stronger than Hβ. Hγ, corresponding to a transition from n=5 to n=2, will be even weaker. [OII] is singly ionized oxygen and when it recombines creates a pair of lines.[4] [OII] is written with brackets because it arises from a forbidden transition, which is a transition with a low probability of occurring. [OIII] is doubly ionized oxygen, with [OIIIb] weaker than [OIIIa], and [NII] is singly ionized nitrogen.

Galaxy spectra are taken by placing a narrow slit across a portion of the galaxy, allowing part of the light to get through. The light then falls on a diffraction grating, which spreads it out into its constituent wavelengths. Light of each wavelength falls onto a particular portion of the CCD (Charged Coupled Device) chip, which records the number of photons received per time. Some spatial information about the object along the length of the slit is recorded, so it is called a 2-D spectrum. The 2-D spectrum for a galaxy is shown in Fig. 3. Markers are set above and below the light from the object to indicate the light that is included in the galaxy spectrum. Everything outside the markers is used as background, which helps to subtract out light coming from the atmosphere. The light between the markers at each wavelength is added up to produce the 1-D spectrum. This removes spatial information. A 1-D spectrum is shown in Fig. 4.

Figure 4: 1-D spectrum of Object 12008948. The dashed lines mark wavelengths of common lines. The blue line is the model galaxy used to calculate the redshift.

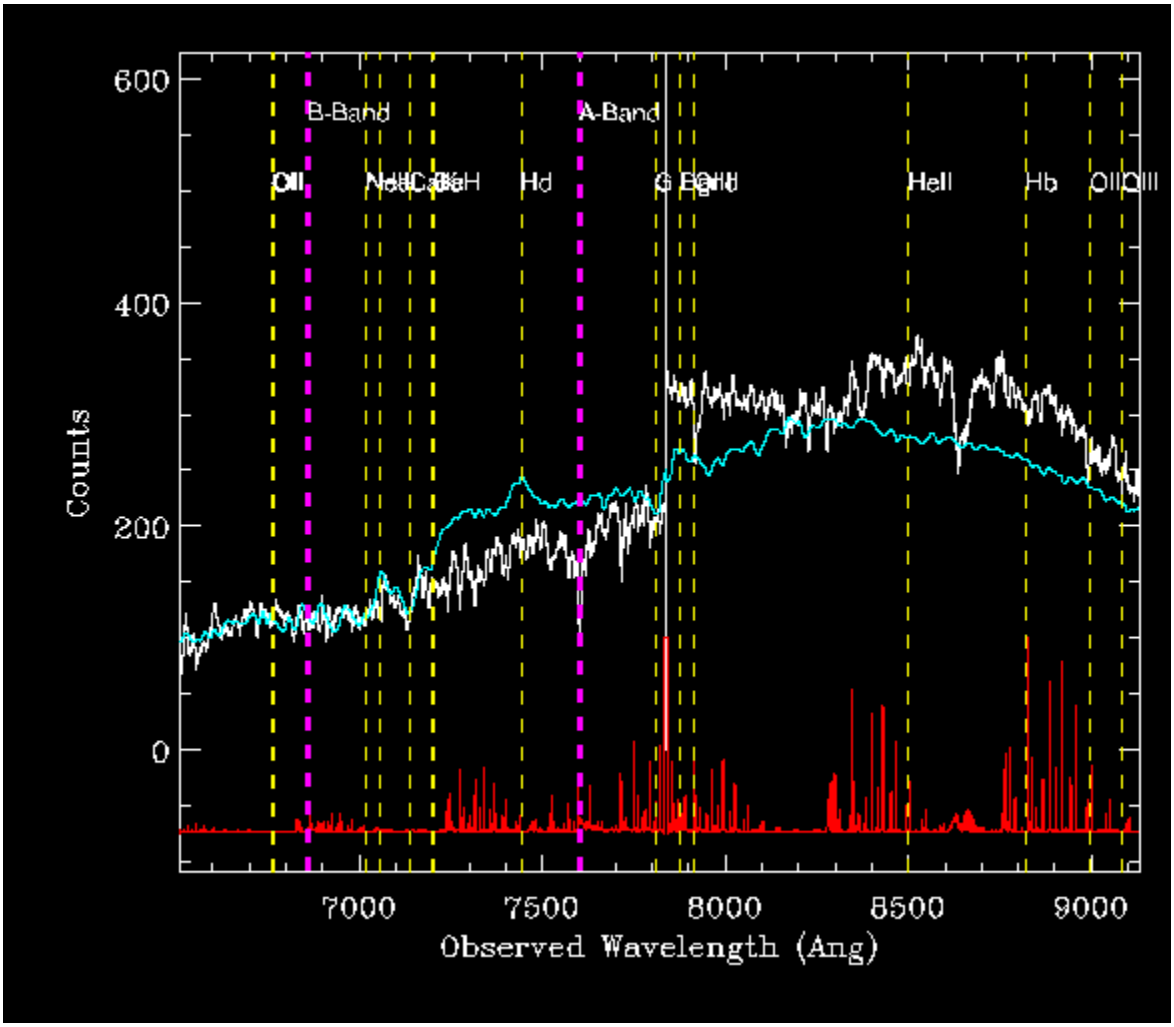

The spectrum for each red sequence object was carefully examined for the presence of any of these lines. Not every spectrum covered the wavelengths of all of these lines, since the rest-frame wavelengths observed by the spectroscope changed with the redshift, but every spectrum covered the wavelength of at least one line. Any that did not were excluded, because there was no way to discern the presence of star formation or AGN. Each 1-D spectrum was ranked according to the likelihood that these emission lines were present. Lines that were significantly stronger than the noise were judged highly likely. Lines that were closer to the level of the noise were judged likely if they were fairly well centered at the expected wavelengths, since it is less likely they would be well centered if not real. Furthermore, the lines must match a certain pattern of intensities (e.g. Hα stronger than Hβ, as described above). Weak lines that were close to the level of the noise or that did not fit the patterns were judged less likely to be legitimate. If there were lines that did not line up with the expected wavelengths, the spectrum was rejected, because these could be from a second galaxy along the line of sight to the intended galaxy from the earth. All the galaxies with probable lines were rejected from the sample. This may have included spectra where the possible lines were purely noise, because the absence of lines was judged very cautiously, to ensure that the sample very likely lacked emission lines.

Occasionally a portion of a galaxy may extend beyond the lines, and there could be emission lines present in this extension . Alternatively, if emission lines are produced by a small clump within the galaxy, they might be swamped by the light from the rest of the galaxy. In either case, the emission lines would not be detected by looking at only a 1-D spectrum. Furthermore, the human eye judges an image such as a 2-D spectrum differently than it judges squiggles on a graph, so it is useful to take a look at the spectrum in an alternative format. For these reasons, the 2-D spectrum of each galaxy whose 1-D spectrum was judged free of lines was examined to look for any missed lines. Out of the 1267 original red sequence galaxies in both the EGS and DEEP catalogs, 411 had no detected emission lines.

Table 3: Information about instruments and bands used. The fourth column contains the wavelength at which light from an object at z∼1 must be emitted to be recorded in the respective bands. NL indicates when the PSF for the band was not listed.

Instrument	Band	Wavelength (μ)	Emitted Wavelength at z∼1	PSF
Spitzer	IRAC 1	3.6	1.8	1.8"
	IRAC 2	4.5	2.25	2.0"
	IRAC 3	5.8	2.9	2.2"
	IRAC 4	8.0	4.0	2.2"
	MIPS 24	23.7	11.9	5.0"
MMT Megacam	u'	0.3551	0.1776	NL
	g'	0.4686	0.2343	NL
	i'	0.7481	0.3741	NL
Subaru Suprime Camera	r'	0.6165	0.3083	NL
CFHT/Megacam	u*	0.37	0.19	<1.1"
	g'	0.485	0.243	<1.0"
	r'	0.625	0.313	<0.9"
	i'	0.770	0.385	<0.9"
	z'	0.885	0.443	<0.9"
CFHT 8Kx12K	B	0.4389	0.2195	1"
	R	0.6601	0.3301	1"
	I	0.8133	0.4067	1"
Palomar/ WIRC	J	1.25	0.625	1"
	K_s	2.14	1.07	1"
AKARI	L15	15.58	7.790	2.3 pix

2.4 Photometry Catalog and SEDs

A Spectral Energy Distribution (SED) is a plot of the flux recorded in each band, appropriately accounting for redshift. To generate an SED for each object, a subcatalog of the EGS catalog was built for the red sequence galaxies without emission lines. There are two populations of galaxies in the subcatalog. One, with non-zero 24μm emissions, will be referred to here as "detected" objects. The other, with no recorded 24μm emission, will be referred to as "non-detected". Table 3 lists the instruments, bands, and wavelengths included in the subcatalog.[8,12]

2.5 Crossmatch Between Bands

The 24μm photometry must be doublechecked, because objects identified at optical and NIR bands may not match up to objects in the 24μm images, for a number of reasons. Some objects are bright at 24μm and dim in optical bands, and some are bright in the optical but very dim at 24μm. The point spread function (PSF) of MIPS at 24μm is larger than the other bands. A PSF describes the way light from a point source is spread out due to the properties of the imaging system.[13] Practically, the PSF affects how close together two objects can be and still be clearly distinguished as separate objects. A large PSF causes several effects, such as that light from a bright object may obscure dimmer objects nearby. Objects closer together than the PSF will look like one object. If this is the case, what appears to be an excess at 24μm would be the combined emission of multiple objects or an object nearby that happens to be bright in this band. The images used to calculate one galaxy's photometry in various bands is presented in Fig. 5. The set of images for each of the 64 galaxies with a non-zero measurement at 24μm were examined to ensure that the objects identified in the optical and NIR bands match the objects identified at 24μm. It was judged a questionable crossmatch if a bright object was too close to the location of the intended object and the target object was close to the level of the noise. In some cases there was no object visible at the supposed location, and in other cases there were two objects in other bands smeared into one object at 24μm. A good crossmatch would be brighter or larger than the noise, not too close to other bright objects in the 24μm image, and have only one object at that location in other bands. Using these criteria, 42% of the crossmatches were considered suspect. This statistic can be used to judge the accuracy of 24μm photometry for further work. After this vetting process, out of the 9253 objects in the DEEP2 redshift catalog with good redshifts, 37 remain that are in the red sequence, have no emission lines, and have good 24μm photometry.

Figure 5: Sample set of multiwavelength images.

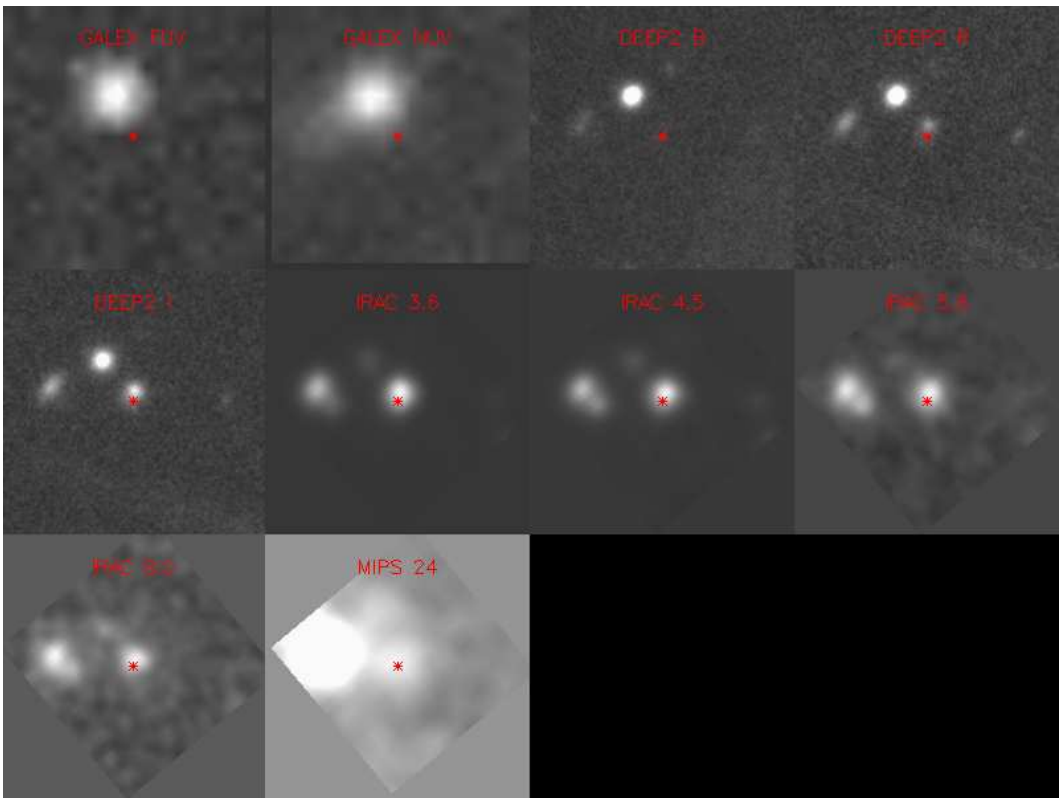

3 Analysis of the Sample

3.1 Color-magnitude diagrams

Color-magnitude diagrams of the detected and non-detected objects are given in Fig. 6. They are divided into the original redshift bins, with the boxes defining the red sequence plotted for reference. The detected objects are plotted in red. There is a clear tendency for the detected objects to be bluer and brighter than the general red sequence, with roughly three-quarters of the detected objects at z>0.4 in this category. This may not be a real trend if only the brightest objects tend to have 24μm emission that is strong enough to detect easily. Thus, a galaxy that is dim overall may have an excess but due to its low luminosity may not be detected by MIPS. The trend with color may be related, since the detector is more sensitive to blue galaxies. Indeed, in the lowest redshift bin, where the lower detector sensitivity to red galaxies does not have much effect, the detected objects are redder than the rest of the RS. However, these objects are still in the brighter half of the RS. To explore whether the trend is just a color and magnitude selection effect, it may prove useful to compare detected and non-detected objects of a similar magnitude, and objects of a similar color, and see what trends remain.

3.2 SED Modelling

An "excess" must be defined relative to some standard. To find the FIR excesses, and to compare the sample objects to galaxies with known properties, theoretical models were used. Model SEDs can be built by adding the predicted emissions of stars, gas, and dust, together with some assumptions about the composition and history of the galaxy. These assumptions include the number of stars, the amount of gas and dust, the metallicity, the initial mass function (the number of stars of each mass that form), and the star formation rate and sequence. Star formation can be modelled as happening in a single burst or gradually over time. Each of these factors is in turn influenced by other factors, such as mergers and galaxy structure. Models can be built with varying levels of complexity. The set of

Figure 6: Color magnitude diagram of 24μ detected objects versus non-detected objects

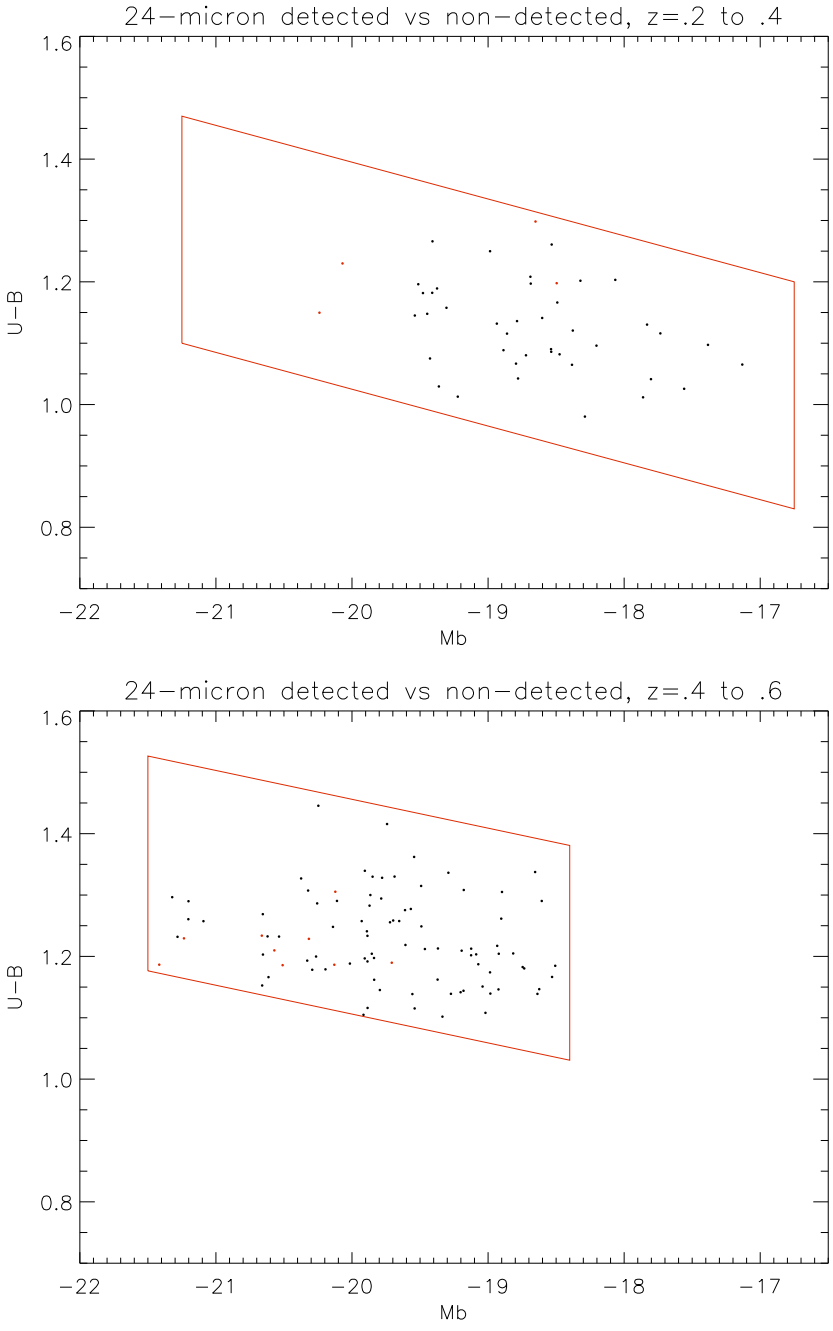

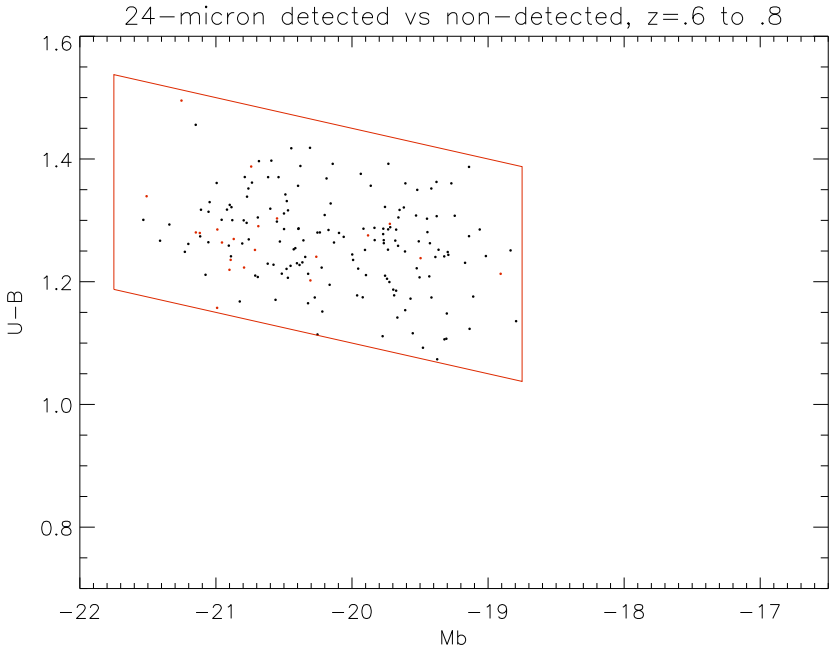
24−micron detected vs non−detected, z=.6 to .8
1.6
1.4
1.2
1.0
0.8
U−B
−22
−21
−20
−19
−18
−17
Mb

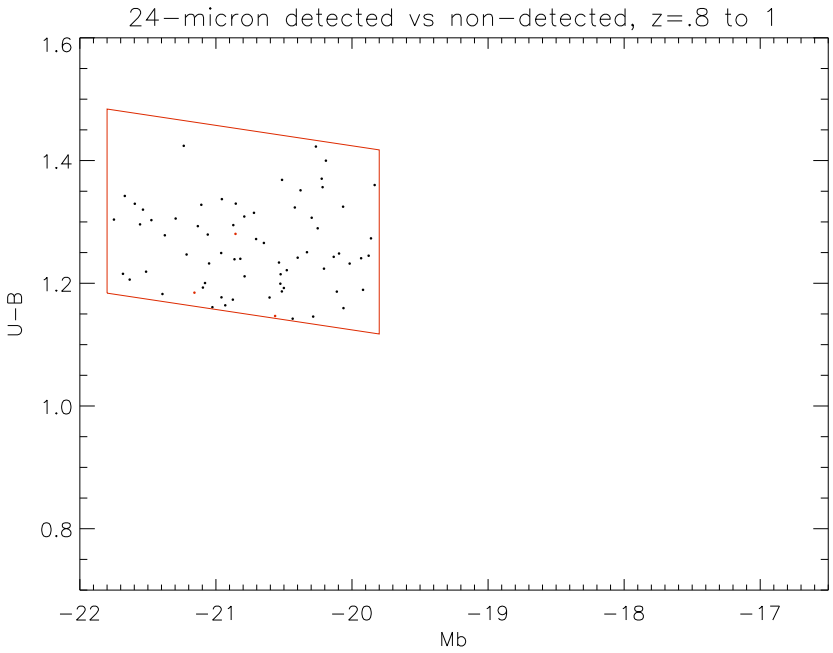
24−micron detected vs non−detected, z=.8 to 1
1.6
1.4
1.2
1.0
0.8
U−B
−22
−21
−20
−19
−18
−17
Mb

templates created by Maraston was used.[14] These templates model SF as an exponentially decaying process with a Salpeter initial mass function, given by

$$\psi(t) = \tau^{-1} e^{-(t/\tau)} \tag{5}$$

$$\phi(m) = m^{-2.35} \tag{6}$$

ψ is the star formation rate, τ is a characteristic "folding time" determining how fast the star formation rate decreases, t is the time since star formation began, ϕ is the proportion of stars formed at a given mass, and m is the initial mass. This is a reasonable picture, as it captures the idea that stars form vigorously while gas is plentiful in the young galaxies, and the star formation rate peters off as gas is used up and blown away by the deaths of the earlier stars. The templates used had a solar metallicity (Z=0.02), with varying age and τ.

Using multi-parameter least squares fitting, each galaxy SED, excluding its MIPS data, was fitted to a template with a particular age and folding time. A band does not record light at only a single wavelength, but instead measures a portion of the photons within a certain range of wavelengths around the central wavelength. To do the fitting, this was taken into account by averaging the template flux over the width of each instrument band, estimated as 0.1λ. The SED and fitted template for each of the detected galaxies is plotted in Fig. 7. One possible trait distinguishing 24μm excess galaxies could be a difference in ages or folding times. Histograms of the fitting results are displayed in Figs. 8 to 11. They are divided into two groups, objects detected and not detected at 24μm. The detected objects have some excess simply by virtue of having a detection, since the predicted 24μm flux is close to the limit of what the instrument could measure. It should also be noted that although the non-detected objects were given a flux of 0 at 24μm, this does not mean that they had no 24μm emission, only that it was too small for the current instrument to reliably detect. The detected objects are on average slightly older, with larger folding times, because the peak of each histogram decays more slowly. The significance of the difference is difficult to judge, because it is a small difference, and the detected group has only 37 objects, compared to

Figure 7: SEDs and fitted Maraston models for the detected objects. The object number and redshift are displayed on each plot.

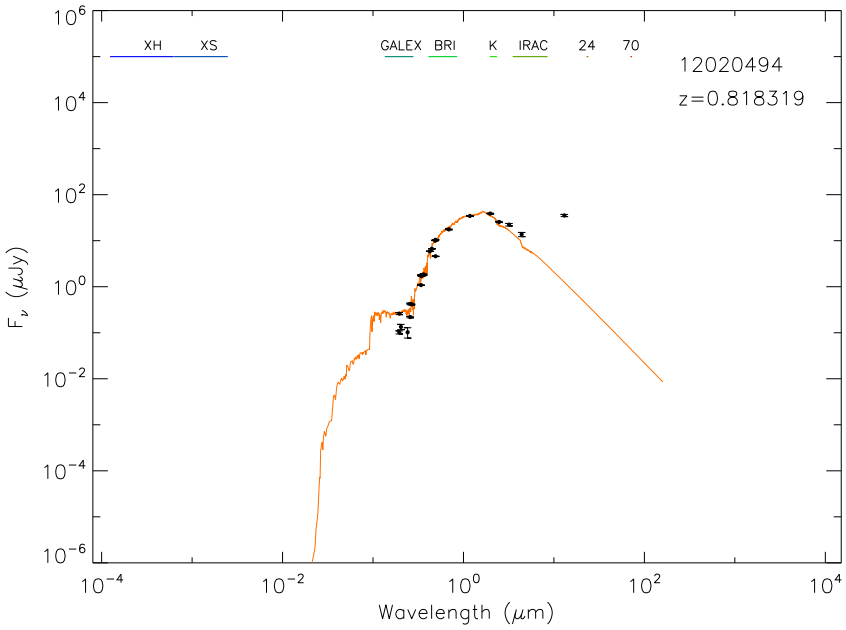

347 non-detected. Thus it may simply be a sampling bias. Further work with larger groups or using objects that are carefully chosen to be similar can help resolve this.

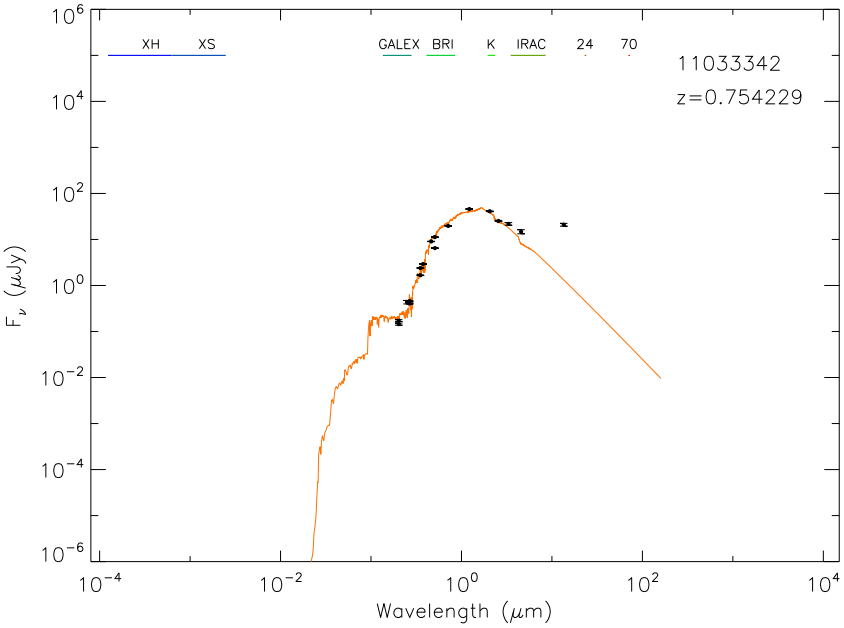
XH
XS
GALEX
BRI
K
IRAC
24
70
11033342
z=0.754229
F_ν (μJy)
Wavelength (μm)

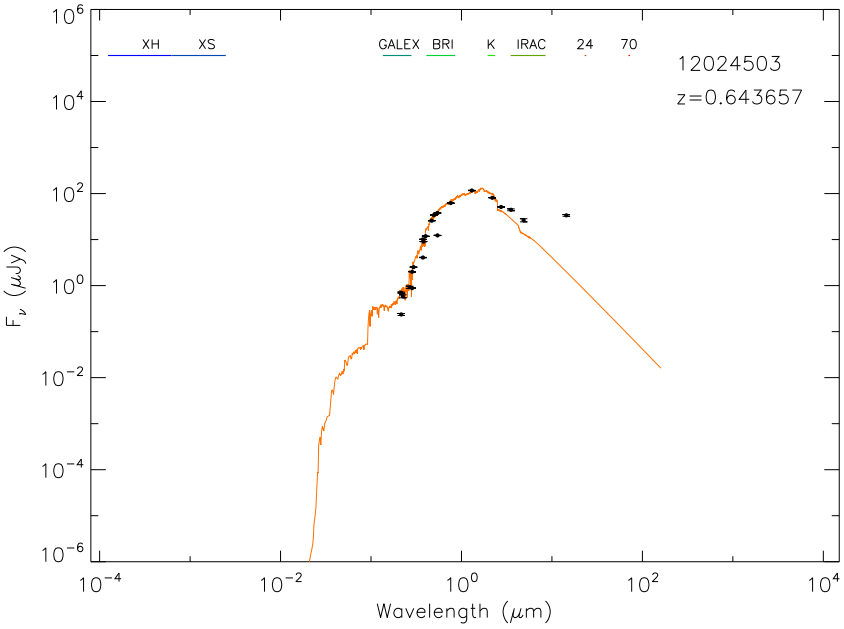
XH
XS
GALEX
BRI
K
IRAC
24
70
12024503
z=0.643657
F_ν (μJy)
Wavelength (μm)

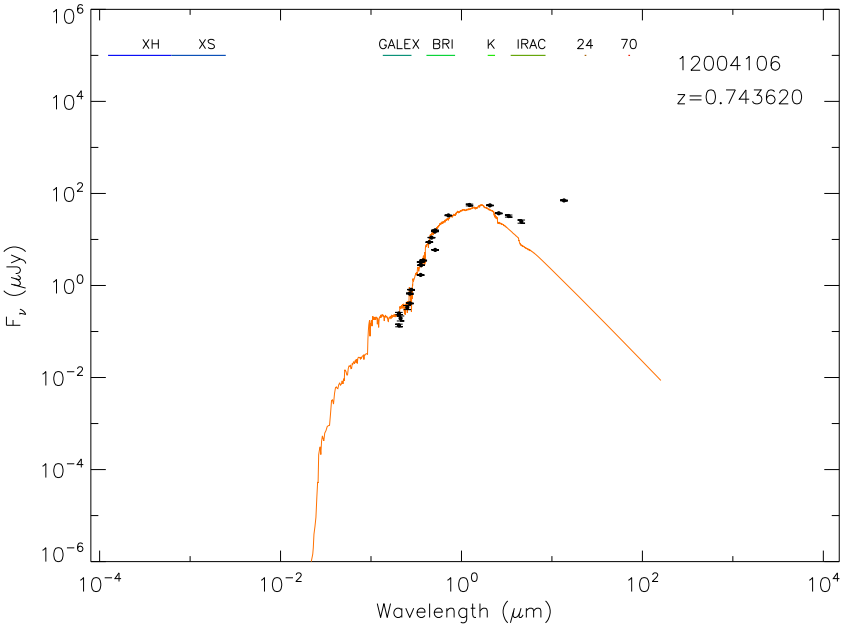
XH
XS
GALEX
BRI
K
IRAC
24
70
12004106
z=0.743620
F_ν (μJy)
Wavelength (μm)

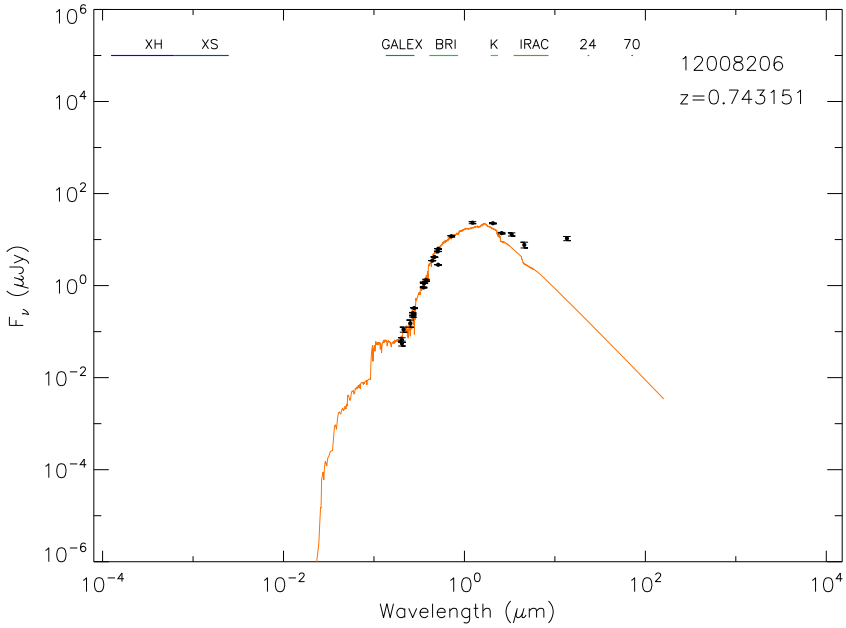
XH
XS
GALEX
BRI
K
IRAC
24
70
12008206
z=0.743151
F_ν (μJy)
Wavelength (μm)

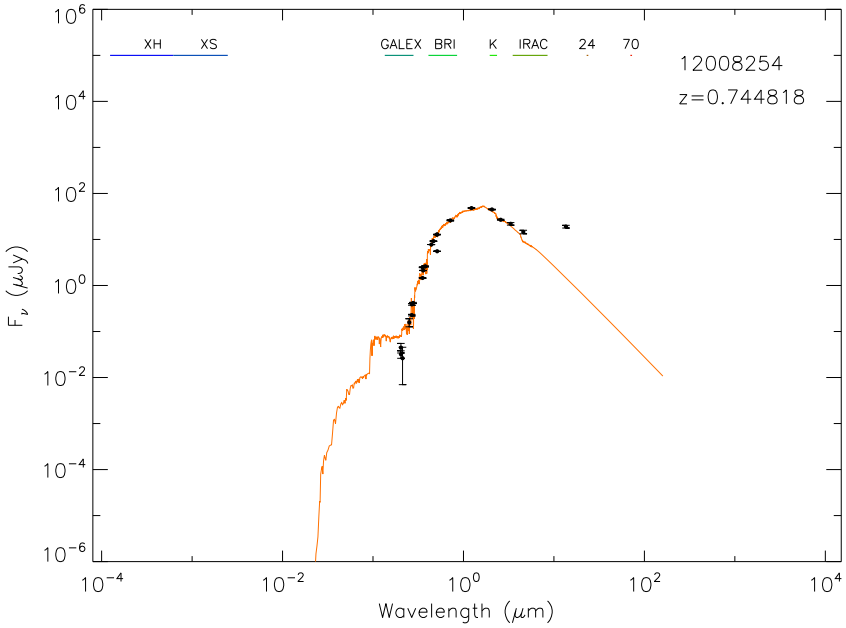
XH
XS
GALEX
BRI
K
IRAC
24
70
12008254
z=0.744818
F_ν (μJy)
Wavelength (μm)

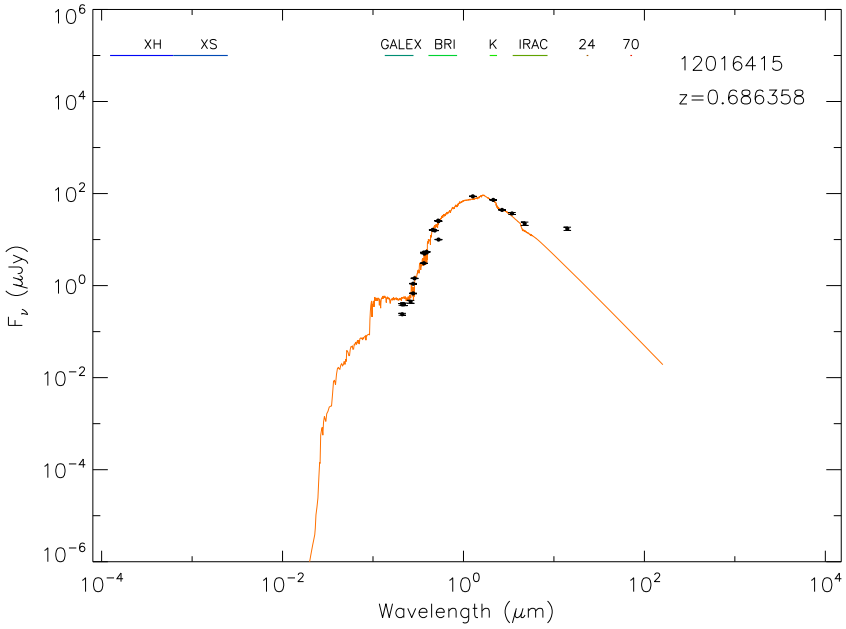
XH
XS
GALEX
BRI
K
IRAC
24
70
12016415
z=0.686358
F_ν (μJy)
Wavelength (μm)

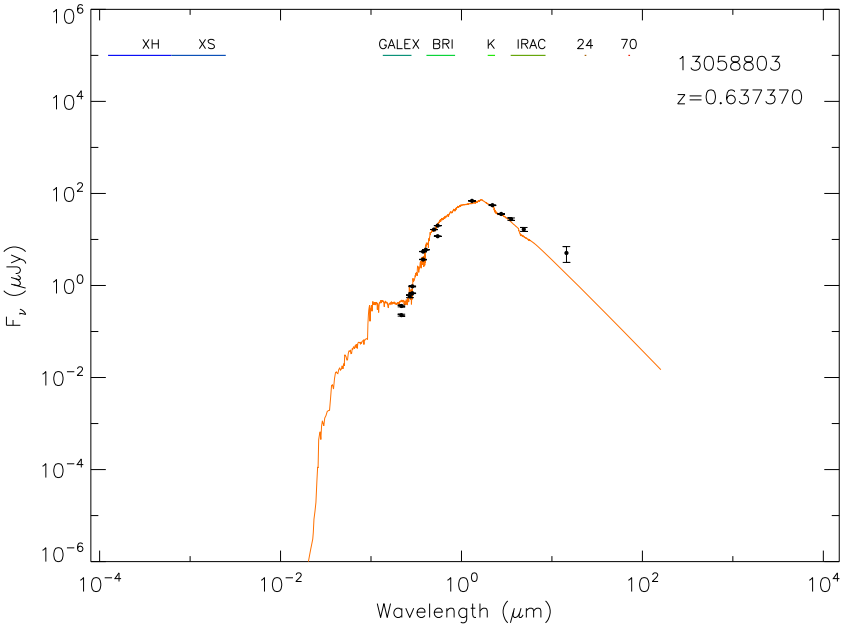
XH
XS
GALEX
BRI
K
IRAC
24
70
13058803
z=0.637370
F_ν (μJy)
Wavelength (μm)

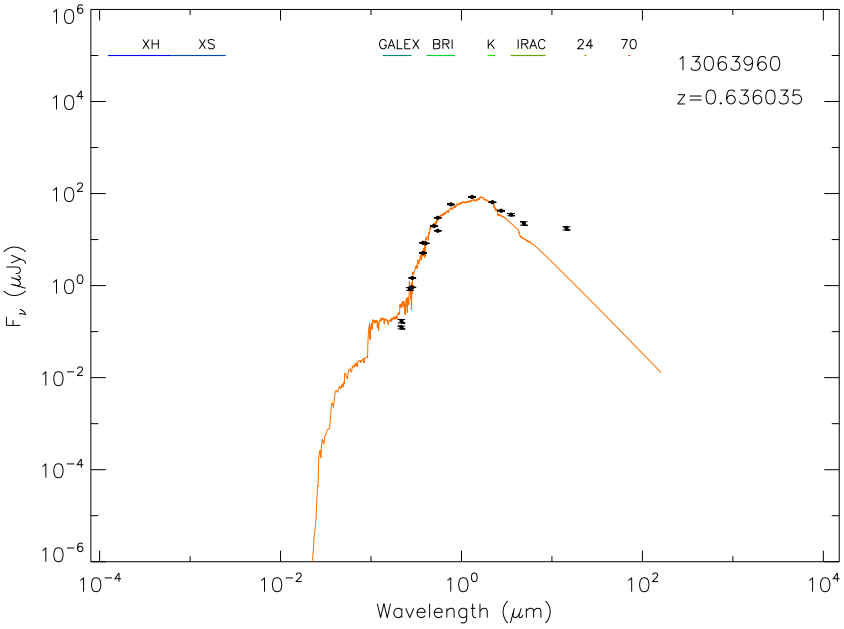
XH
XS
GALEX
BRI
K
IRAC
24
70
13063960
z=0.636035
F_ν (μJy)
Wavelength (μm)

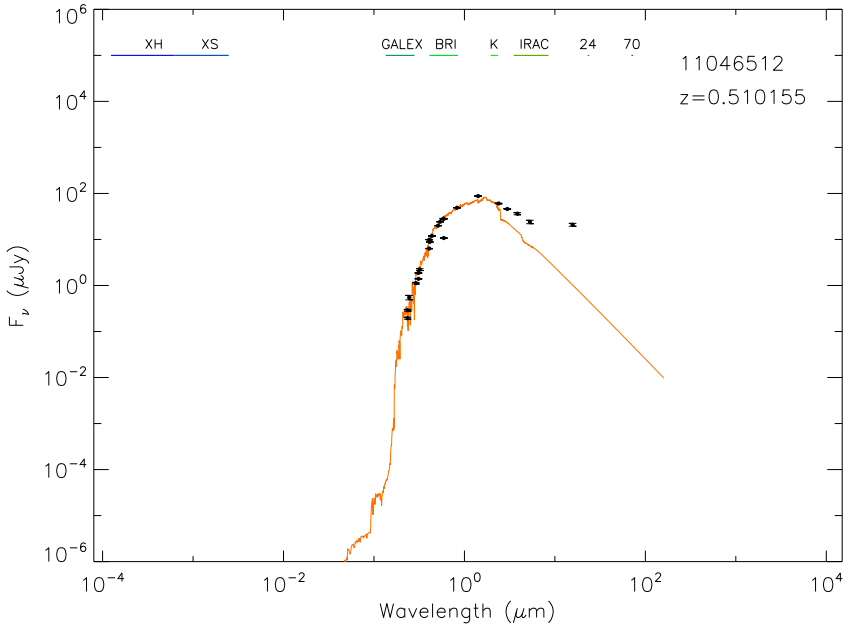
XH
XS
GALEX
BRI
K
IRAC
24
70
11046512
z=0.510155
F_ν (μJy)
Wavelength (μm)

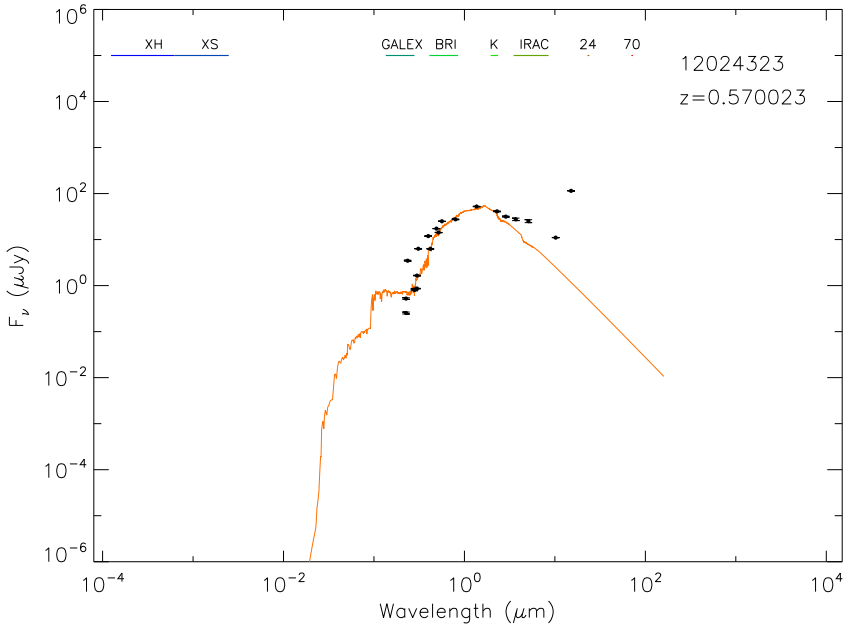
XH
XS
GALEX
BRI
K
IRAC
24
70
12024323
z=0.570023
F_ν (μJy)
Wavelength (μm)

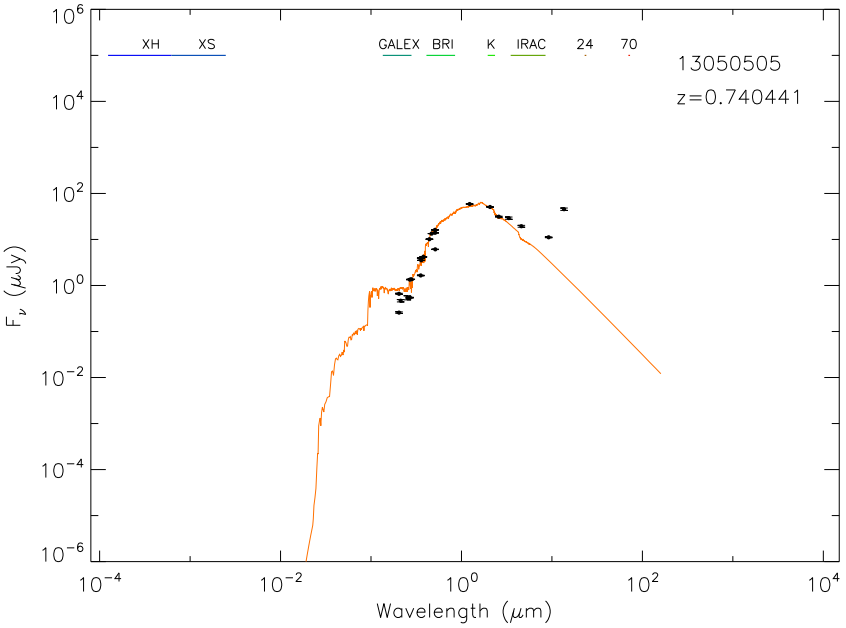
XH
XS
GALEX
BRI
K
IRAC
24
70
13050505
z=0.740441
F_ν (μJy)
Wavelength (μm)

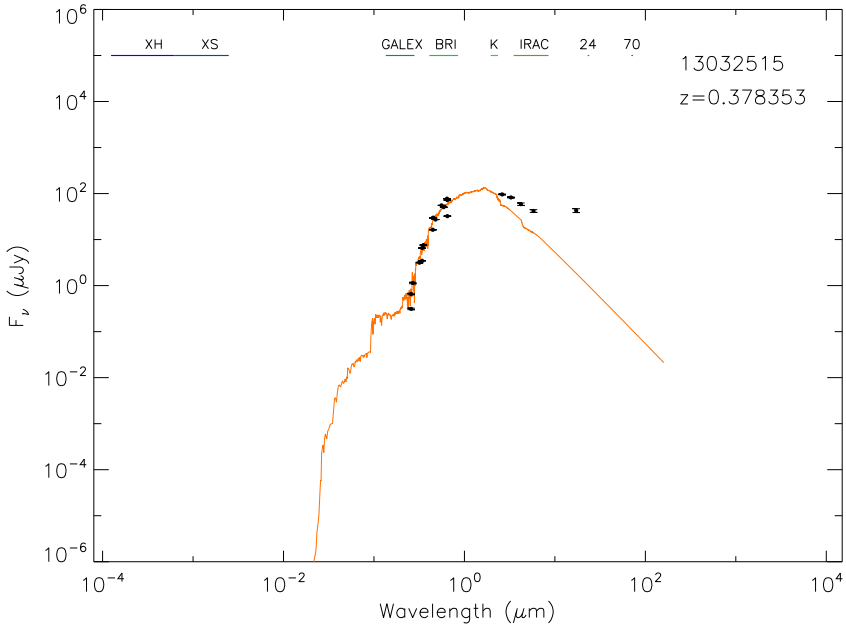
XH
XS
GALEX
BRI
K
IRAC
24
70
13032515
z=0.378353
F_ν (μJy)
Wavelength (μm)

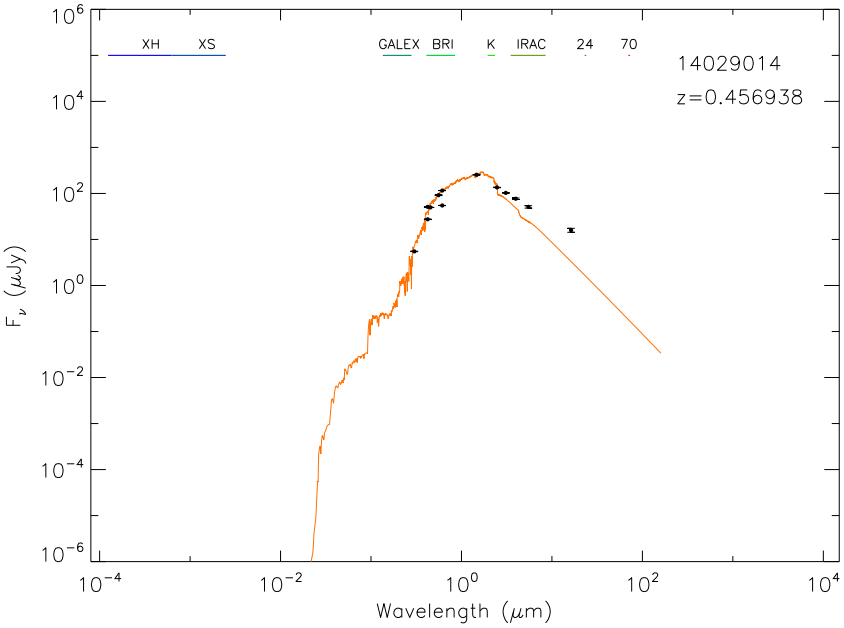
XH
XS
GALEX
BRI
K
IRAC
24
70
14029014
z=0.456938
F_ν (μJy)
Wavelength (μm)

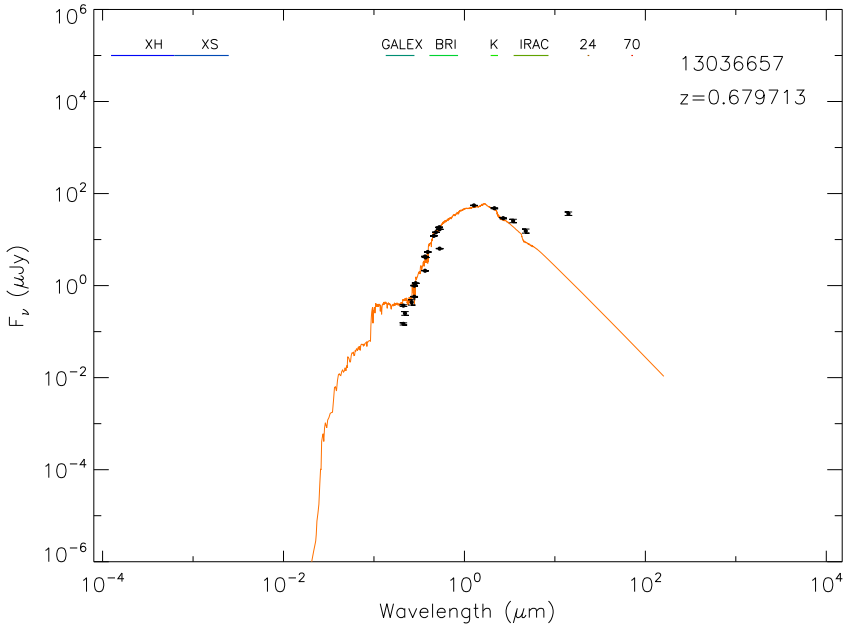
XH
XS
GALEX
BRI
K
IRAC
24
70
13036657
z=0.679713
F_ν (μJy)
Wavelength (μm)

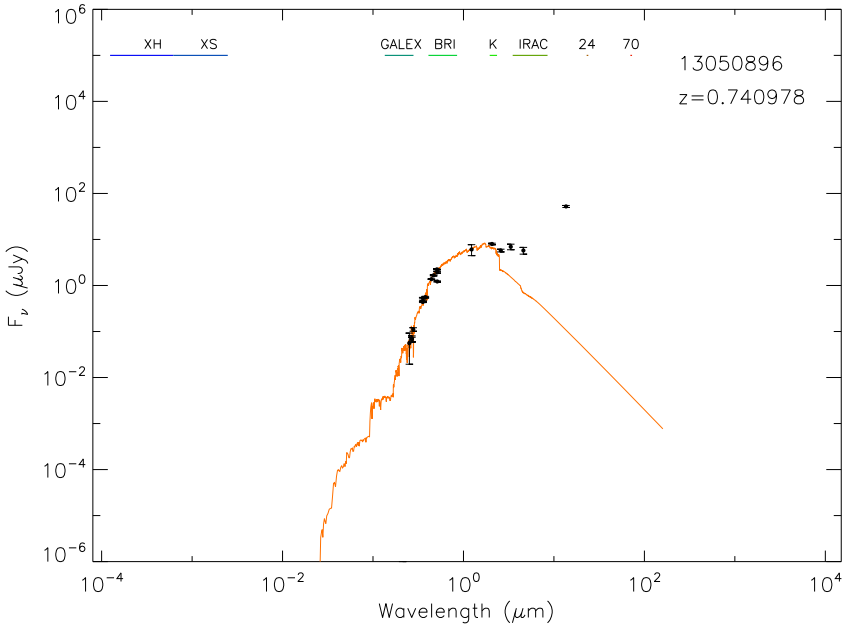
XH
XS
GALEX
BRI
K
IRAC
24
70
13050896
z=0.740978
F_ν (μJy)
Wavelength (μm)

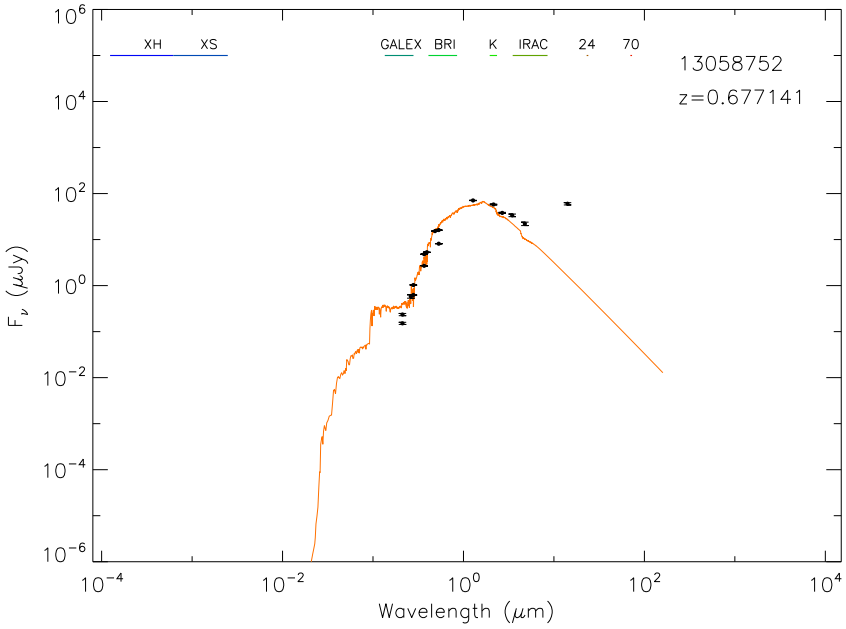
XH
XS
GALEX
BRI
K
IRAC
24
70
13058752
z=0.677141
F_ν (μJy)
Wavelength (μm)

.

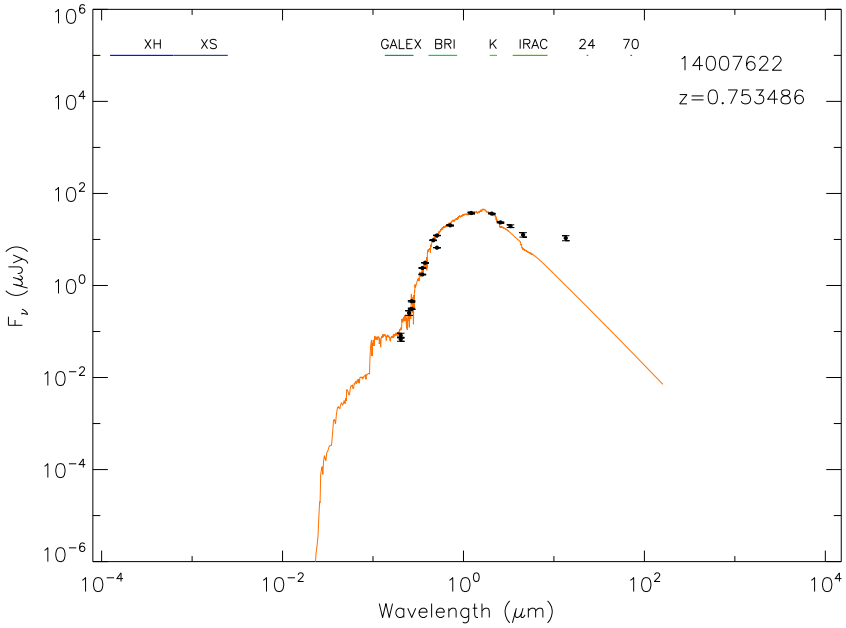
XH
XS
GALEX
BRI
K
IRAC
24
70
14007622
z=0.753486
F_ν (μJy)
Wavelength (μm)

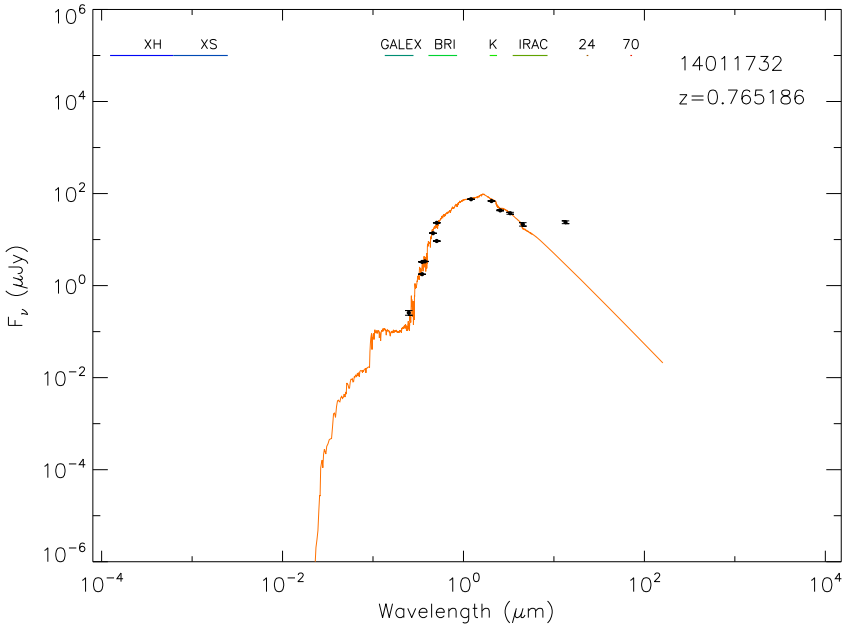
XH
XS
GALEX
BRI
K
IRAC
24
70
14011732
z=0.765186
F_ν (μJy)
Wavelength (μm)

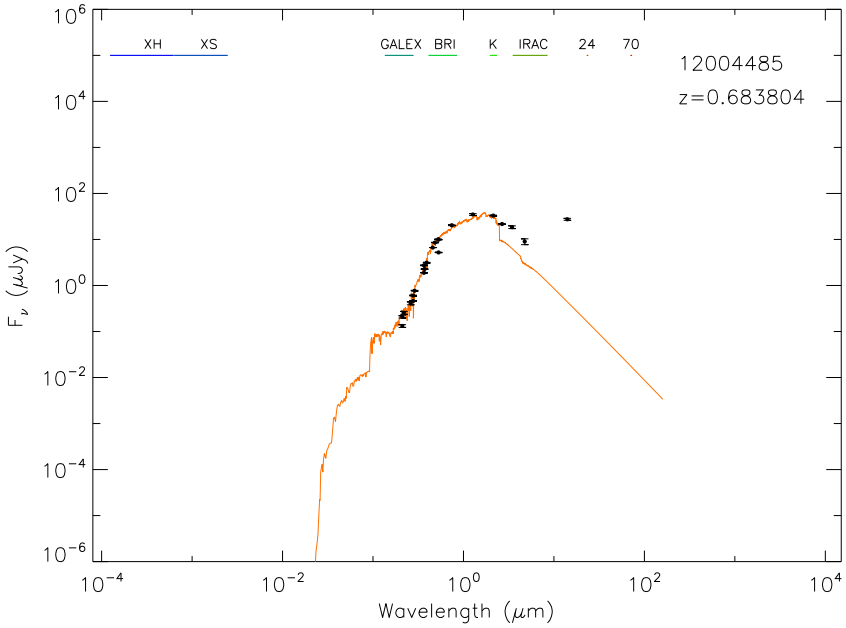
XH
XS
GALEX
BRI
K
IRAC
24
70
12004485
z=0.683804
F_ν (μJy)
Wavelength (μm)

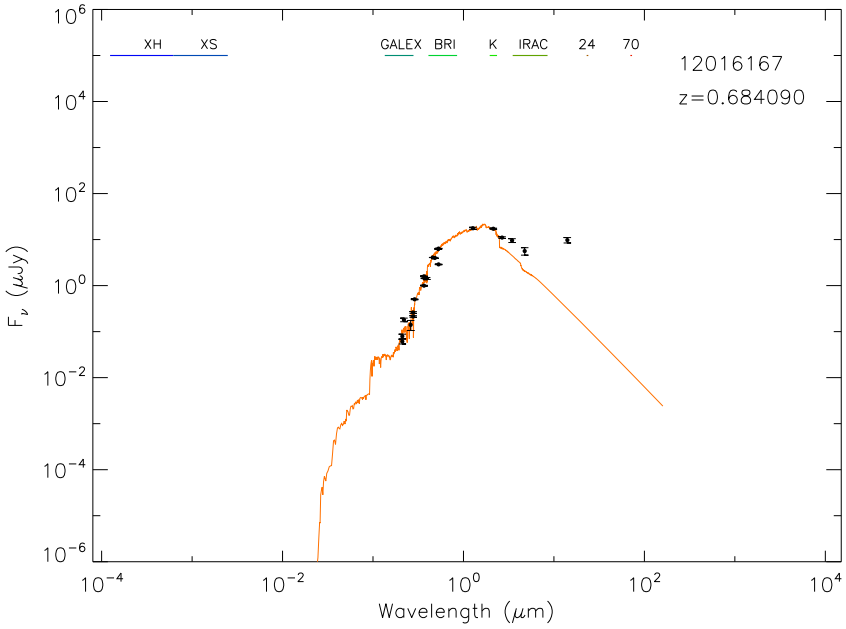
XH
XS
GALEX
BRI
K
IRAC
24
70
12016167
z=0.684090
F_ν (μJy)
Wavelength (μm)

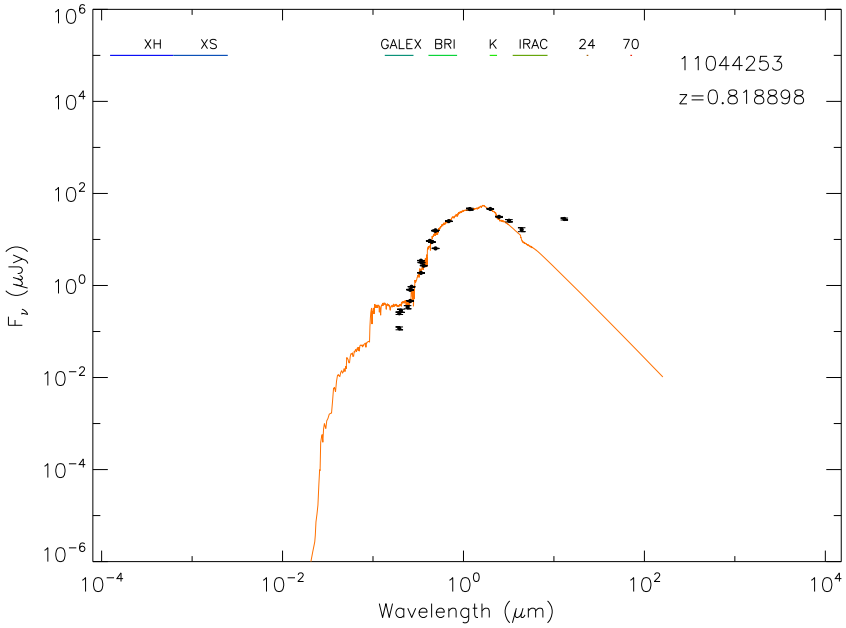
XH
XS
GALEX
BRI
K
IRAC
24
70
11044253
z=0.818898
F_ν (μJy)
Wavelength (μm)

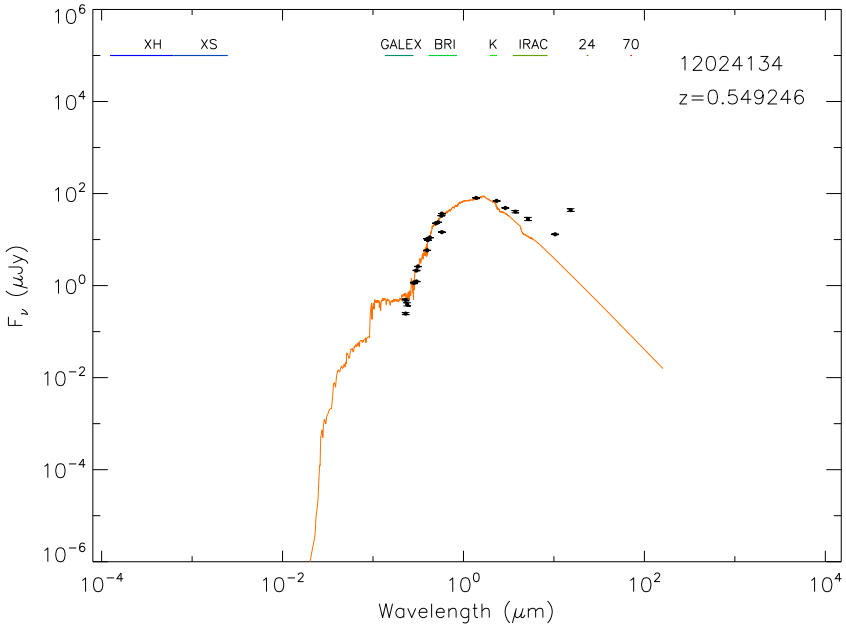
XH
XS
GALEX
BRI
K
IRAC
24
70
12024134
z=0.549246
F_ν (μJy)
Wavelength (μm)

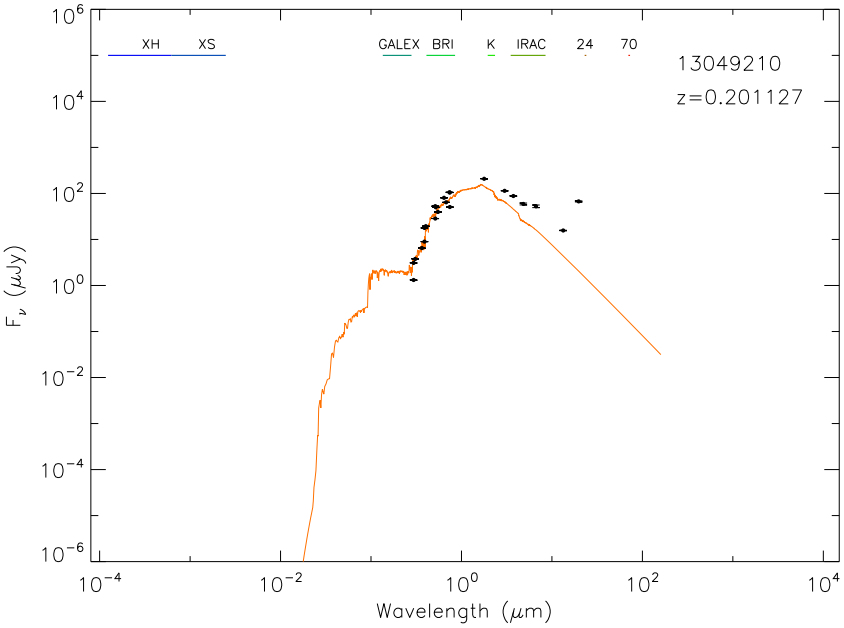
XH
XS
GALEX
BRI
K
IRAC
24
70
13049210
z=0.201127
F_ν (μJy)
Wavelength (μm)

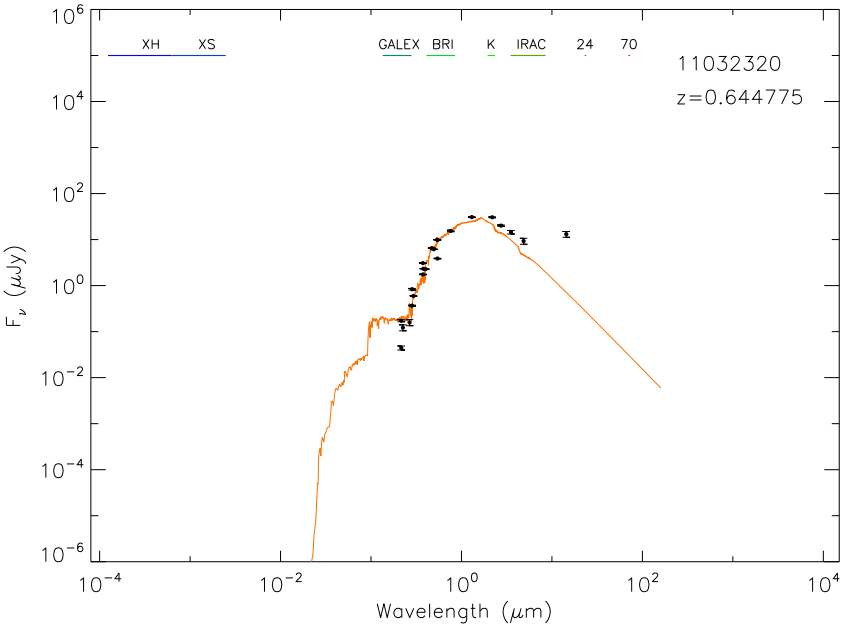
XH
XS
GALEX
BRI
K
IRAC
24
70
11032320
z=0.644775
F_ν (μJy)
Wavelength (μm)

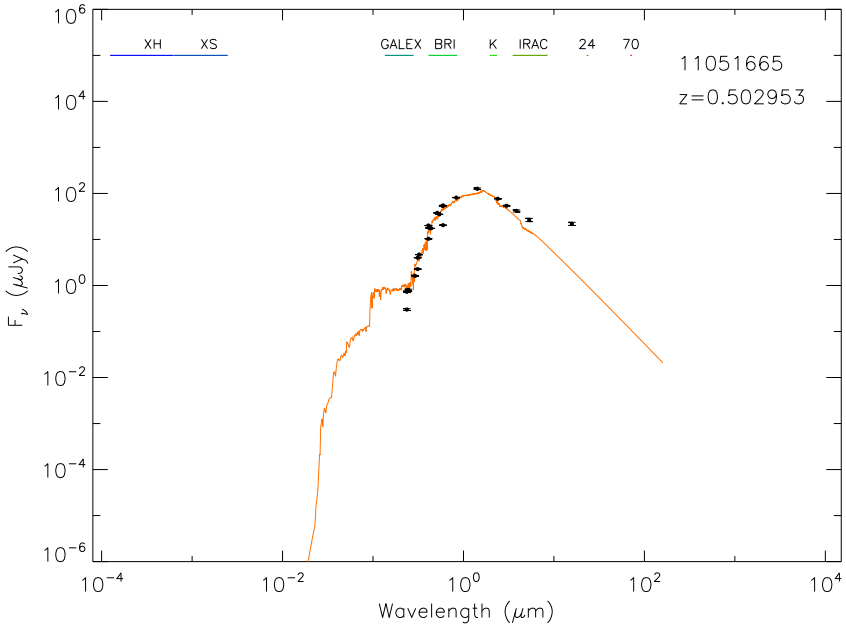
XH
XS
GALEX
BRI
K
IRAC
24
70
11051665
z=0.502953
F_ν (μJy)
Wavelength (μm)

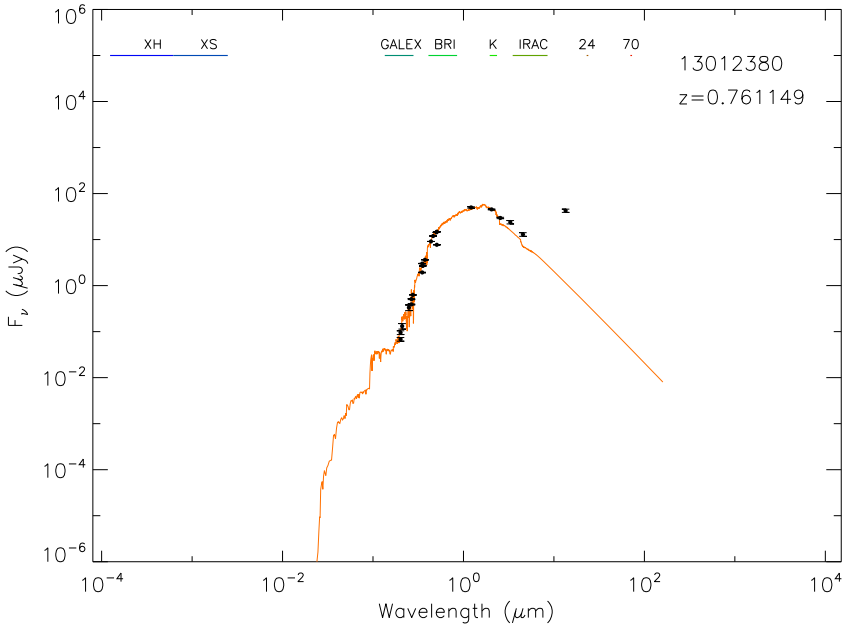
XH
XS
GALEX
BRI
K
IRAC
24
70
13012380
z=0.761149
F_ν (μJy)
Wavelength (μm)

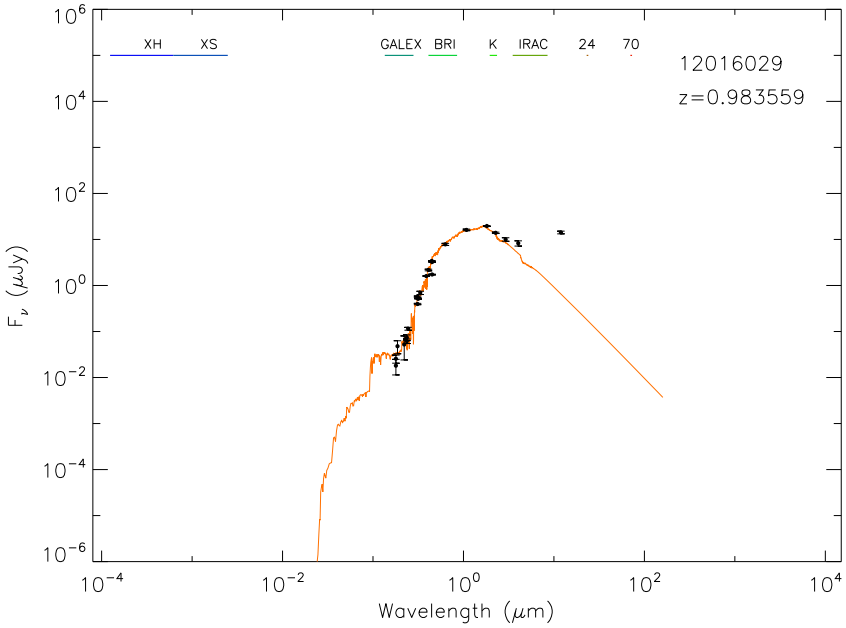
XH
XS
GALEX
BRI
K
IRAC
24
70
12016029
z=0.983559
F_ν (μJy)
Wavelength (μm)

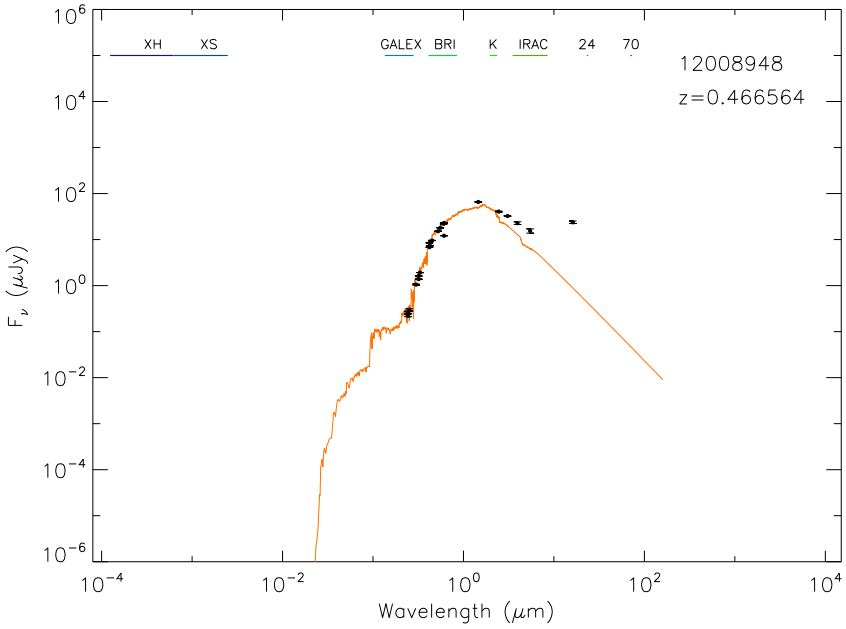
XH
XS
GALEX
BRI
K
IRAC
24
70
12008948
z=0.466564
F_ν (μJy)
Wavelength (μm)

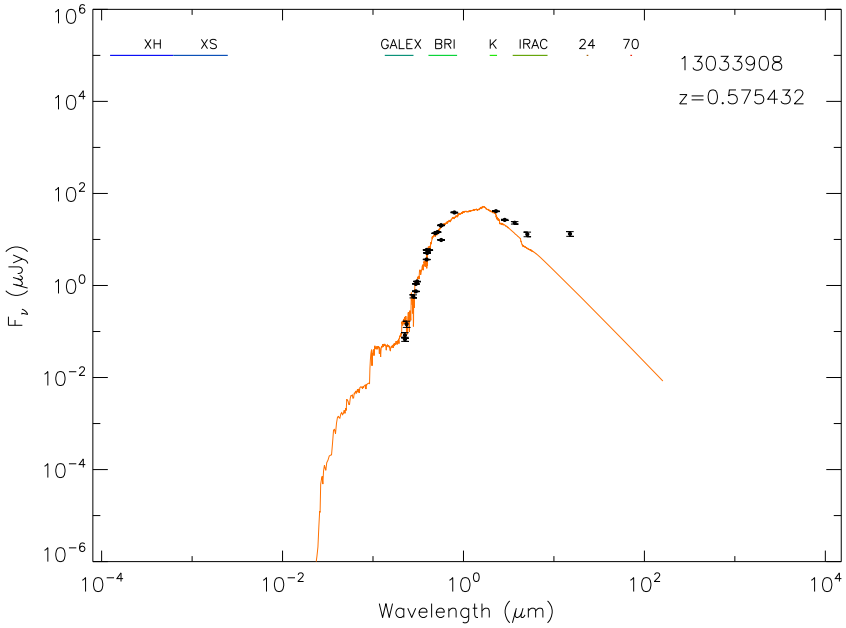
XH
XS
GALEX
BRI
K
IRAC
24
70
13033908
z=0.575432
F_ν (μJy)
Wavelength (μm)

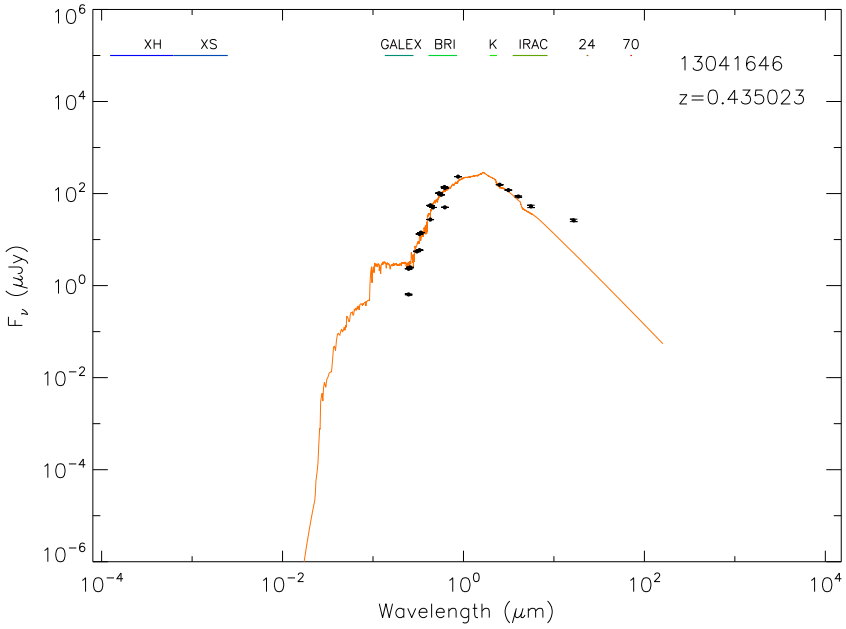
XH
XS
GALEX
BRI
K
IRAC
24
70
13041646
z=0.435023
F_ν (μJy)
Wavelength (μm)

Figure 8: Histogram of calculated ages of non-detected objects

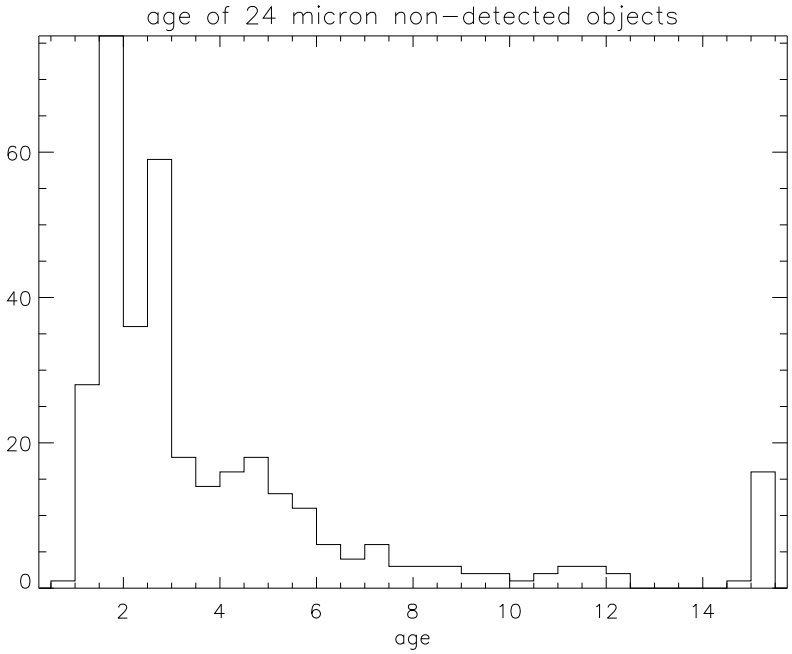

Figure 9: Histogram of ages of 24μm detected objects.

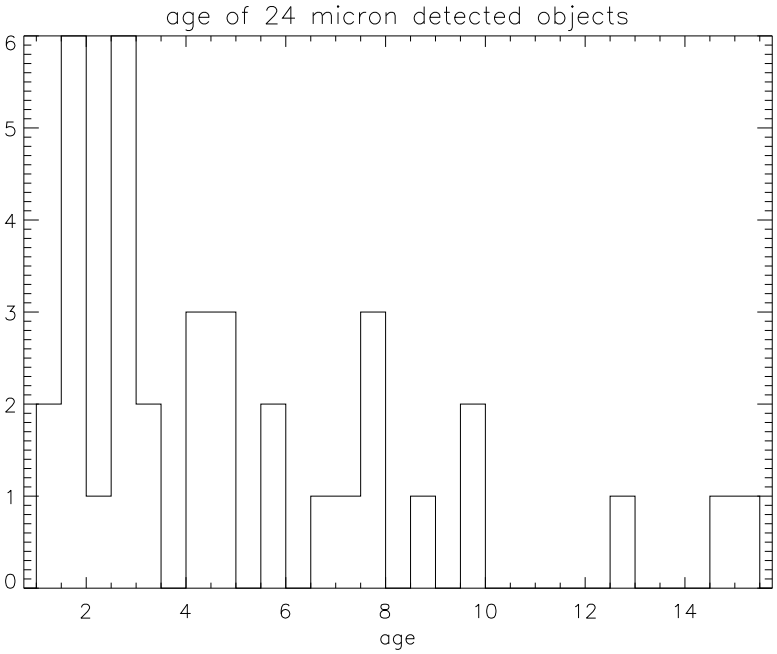

Figure 10: Histogram of τ's of non-detected objects.

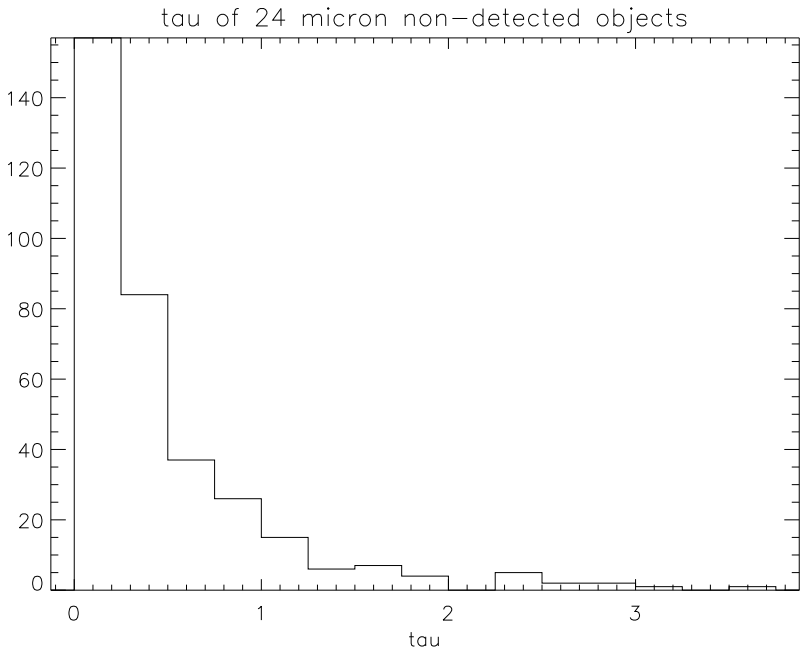

Figure 11: Histogram of τ's of detected objects.

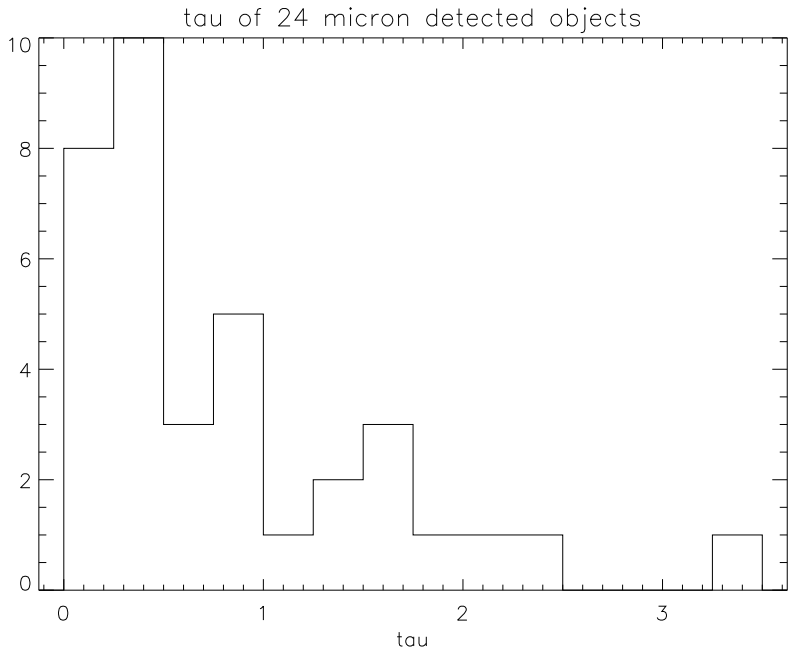

3.3 Color images

Simply looking at images of these objects can provide insight into their nature. Sixteen of the detected objects had images taken by the Hubble Space Telescope ACS, in its F606W and F814W bands. The images of each object in these two bands were averaged together to create a third image of an intermediate color. To create the color images, these three images were combined to build red-green-blue triplets corresponding to various colors, depending on the amount of each component color in the triplet. The images were scaled to determine the strength of each component image in the final color image. The scaling was chosen by eye so that there was good contrast between colors, while still retaining a naturalistic look.

The color images for the detected objects, and for a representative sample of non-detected objects are shown in Figs. 12-15. The redshifts of the two groups were chosen to be

Figure 12: 24μm detected objects, in order of redshift. The DEEP objects numbers and redshifts are given for each.

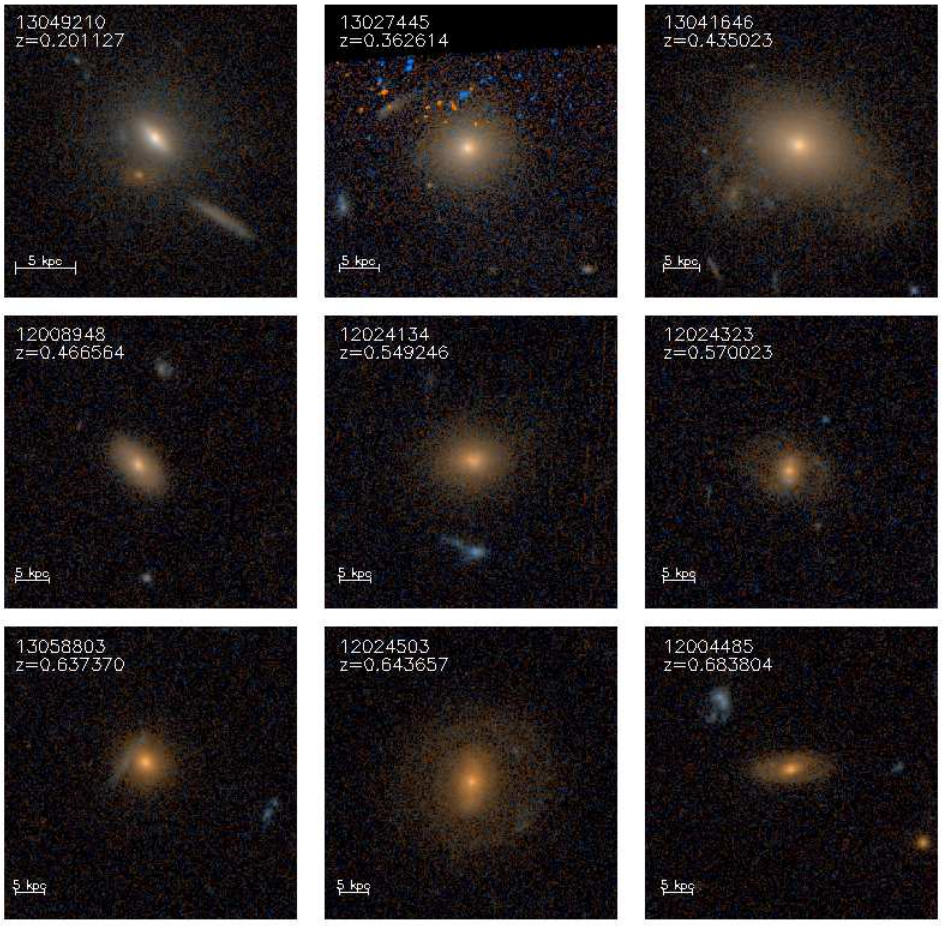

Figure 13: Images of 24μm detected objects

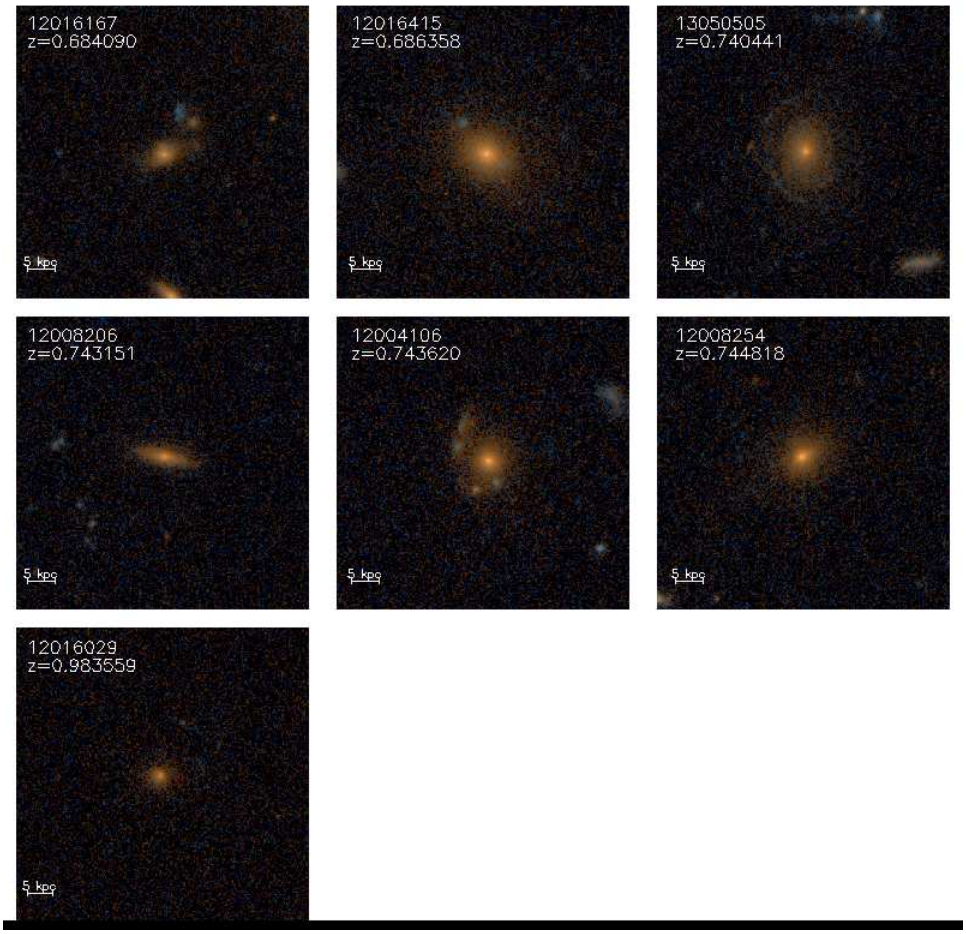

Figure 14: 24μm non-detected objects. Each object has a similar redshift to the corresponding image in the previous two figures.

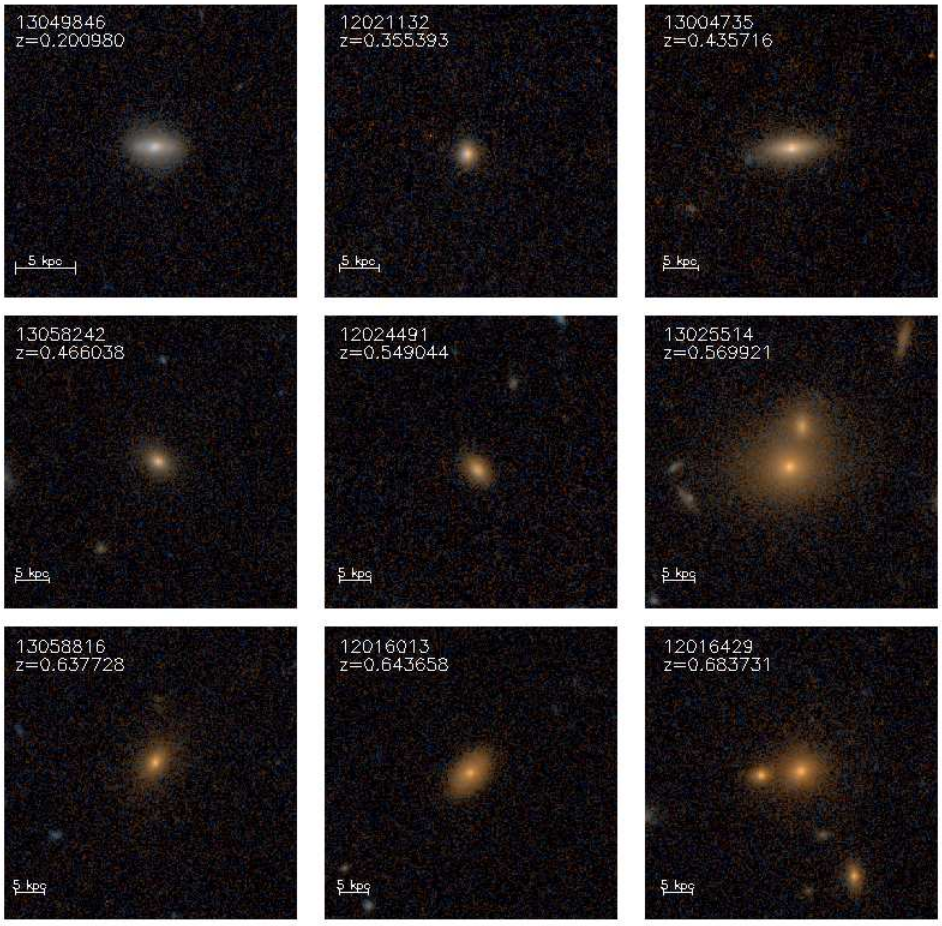

Figure 15: 24μm non-detected objects.

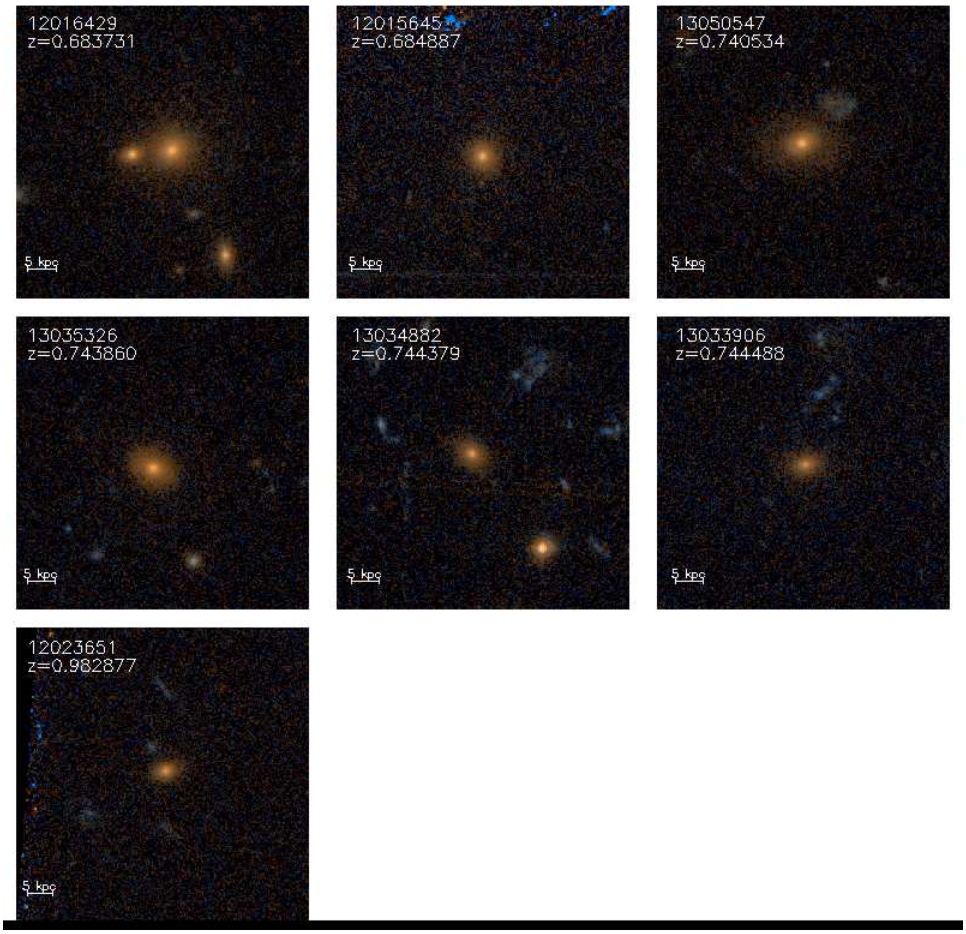

similar, because galaxies at a larger redshift will appear smaller and redder than the same galaxy close by. Examining the two sets of images, it is clear that the detected galaxies more often have blue portions or a disturbed morphology than the standard red sequence comparison galaxies. Table 4 presents a summary of the visual properties of each sample galaxy, compared to a galaxy at a similar redshift that does not have 24μm emission. Each pair is composed of one object from the detected sample, and one non-detected object. Thus, the first object from Fig. 12 is compared to the first object in Fig. 14. In the table, I considered clumps of blue within about half the radius of the galaxy in question to be possible sources of confusion. In some cases it is difficult to tell if these clumps of blue are the source of the emission or part of the galaxy. They may be foreground or background objects, the remnants of cannibalized galaxies, or even gravitational lensing of another object. Many of the images had some blue clumps farther from the central galaxy. Of the sample objects, 13 had blue clumps within about one diameter of the object, and 14 had definite blue clumps within the image. Of the comparison objects, 7 had blue clumps within one diameter, and 11 had blue clumps within the image. These numbers are not meant to be definitive, but only to give some grounds for quantitative comparison. There is a clear tendency for detected objects to have more blue present. Relative size was judged by eye. The sample object was considered larger if its area on the image was significantly larger. If the difference in size was small and harder to judge, it was labeled "similar". "Structure" here can refer to possible spiral arms, a clump of gas, a possible dust lane, or less well defined differences in appearance from a simple spheroid. In the context of these images, it indicates a fairly abrupt change in brightness or color in the object that gives the appearance of physical structures. In addition to real structures in the gas and stars, these appearances can be an effect of the orientation of the galaxy or superimposed objects. I have made no systematic attempt to classify the structure physically, except to note when it seems likely to indicate a disk. "Multiple Objects" may or may not be physically related, but may simply be superimposed. Some (e.g. object 12004106) seem highly likely to be a real association, whereas others (e.g. 13058803) may be coincidental. Without further

information on these companions, it is difficult or impossible to know for certain. The blue suggests star formation, and the disturbed morphology suggests a recent merger with another galaxy. Hubble images were not available for all of the objects, but it can be posited that they would have similar features.

4 Discussion

The clearest pieces of evidence for the cause of the excess are the CM diagrams and the color images. They both suggest that these objects are bluer than the average red sequence. This may indicate that the excess was caused by star formation that was not detected with emission lines. The question then arises of why the emission lines were not observed. One possibility is that the lines were weak enough to be overlooked. Examining the CMDs, there are fewer red sequence galaxies without emission lines between z$\sim$0.2 and z$\sim$0.4 (45, compared to 65 for 0.8$<$z$\lesssim$ 1.0), despite the greater completeness. This may indicate that emission lines were more easily detected in nearby, and thus brighter, galaxies. If so, the lines were missed in some fraction of more distant objects. This may be due to the lower signal to noise ratio for dimmer objects. Stacking subsamples of spectra, for instance the spectra of galaxies with a 24μm detection in each redshift bin, would further test this, since stacking improves the signal to noise ratio.

The ACS images suggest another possibility. The clumpiness of the blue light is significant, because the slit is narrow and only covers part of the galaxy. A single clump of SF close to the galaxy could easily be missed by the spectroscope, while being included in the MIPS photometry. A few objects, e.g. 13004735, have a blue clump close to the object, and yet have no detection by MIPS, complicating this clean interpretation. The presence of blue clumps within various radii of the central object could be characterized more rigorously, by counting blue pixels within various annuli, instead of judging this roughly by eye. The 24μm detected objects were on average larger, and since the width of the annuli was based on object size, the count of blue clumps may have been increased for the detected objects.

Table 4: Summary of image properties.

Pair No.	DEEP Object Number	Size	Color	Other Comments
1	13049210	main object similar; multiple objects	small blue clump, external red object	
	13049846			possibly some structure
2	13027445	larger	similar	
	12021132			possible dust reddening
3	13041646	larger	external blue spiral structure	possible structure in extended weak emission
	13004735		blue clump	
4	12008948	larger		
	13058242			
5	12024134	larger		some structure near nucleus
	12024491			
6	12024323	similar	blue clumps	definite structure, possible arms, ring around nucleus
	13025514			two objects
7	13058803	larger	blue streak	
	13058816			
8	12024503	larger	blue clumps	definite structure, possible spiral arms
	12016013			
9	12004485	larger	blue clumps	disk, possible ring
	12016429			multiple objects
10	12016167	similar	blue clump	multiple objects
	12016429			two objects
11	12016415	larger	blue clumps	
	12015645			
12	13050505	larger	blue rings	rings
	13050547			external blue object; extended faint emission
13	12008206	similar		possible disk
	13035326			
14	12004106	larger	blue clumps	clumps in an arc
	13034882			
15	12008254	larger		
	13033906			
16	12016029	smaller		
	12023651		blue clump	

As the radius gets larger, regardless of the size of the object, more blue clumps that are not physically connected to the central object will be included. On the other hand, objects that are larger will have larger spheres of influence, and more of the bits of blue may be physically associated with it. This is important to understanding the physics of the galaxies. However, regardless of the physical relations, the clumps of young stars could explain 24μm emission without emission lines. Currently, each detected object that had a Hubble picture was compared to a single non-detected object. The detected objects were twice as likely to have blue light close by, which is a large enough difference that it is unlikely to be purely chance. However, to robustly examine the significance of this result, and to get a sense of how the detected objects compare to a typical galaxy at that redshift, a larger sample would be useful. The supply of 24μm detected objects is very limited, but there are many more non-detected objects. A collection of these objects would give an indication of the average appearance of red sequence galaxies near a given redshift.

Before examining the SEDs, a short discussion of the relationship between age, τ, and galaxy photometry will prove helpful. Just as for spectra, the SED demonstrates the combined effects of the young and old stars, gas, dust, and possibly AGN making up the galaxy, with each component affecting the light in each band differently. As discussed before, younger stars emit strongly in shorter wavelengths. This light may be absorbed and reemitted in the IR. Young galaxies also have more gas and a lower metallicity and dust content, and thus are less reddened. Dust obscures the optical bands, especially bluer wavelengths. It blocks little of the light at 8μm, so this band is composed of mainly stellar emission. SF and AGN would create a spike at 24μm, instead of the decline typically observed when they are absent. As a galaxy ages, its short wave radiation decreases, while the NIR radiation grows as it is dominated by the light from older stars.[2] When t is small, the star formation rate will be high, so that many young stars are present. A small τ corresponds to a burst of star formation early on that quickly dies off, while a large τ corresponds to less intense star formation dying off very slowly. Thus, for a large τ , with fewer stars forming during a given epoch, star formation will continue at a higher level for a longer period of time. With

a small τ, or t much larger than τ, the light from old stars will dominate, producing a bump in the UV and the NIR.

Most of these SEDs share a characteristic shape, with a hump centered in the NIR, and declining in the MIR. Every object had at least some excess at 24μm, and most had a fairly substantial excess (about a factor of 10 or more in excess). Every object having some excess may be due to the cutoff limit for MIPS detection, as remarked earlier. The large excesses would not be explained by this, and require another explanation. A larger folding time hints at a younger stellar population for the detected objects, favoring ongoing star formation. A fair number of the SEDs had a bump in the NIR, which could possibly be due to old stars. If so, diffuse dust heated by the UV from the old stars could explain the excess. This is supported by the larger average age of these objects. A direct comparison of the calculated age, τ, and the SED for each object would test this. However, the ages and τ's provide ambiguous evidence, and normalizing the histograms to the same level would make it easier to compare the two groups. There is still the question of why the model did not fit in the NIR for these objects, despite fitting the optical bands well. It could be due to a poor fit, or a lack of a template with the exact age and τ needed to match the data. If the bump is real, because the model did not include the effect of dust, mergers, or AGN, a discrepancy between the model and the data may be an indication that something beyond simple stellar evolution is occurring. Another poor fit occurs for some of the SEDs on the short-wavelength end, possibly due to attenuation by dust. It may be illuminating to examine the ages and τ's for the objects showing these fit discrepancies, to see if there is a trend.

5 Conclusion

5.1 Further Work

Much work remains to firmly establish the cause of the FIR excess. I plan to stack the spectra of detected and non-detected objects to further test whether the detected objects

are truly free of emission lines. If any weak lines were found, line strength ratios and widths could be measured to determine if they were produced by SF or an AGN. My next step will be to calculate the amount of excess by subtracting the template flux within the 24μm band from the observed emission, and plotting the residuals between the fit and the data. This work until now has been focused on averages, but for such a small number (37) it is possible to inspect each individually. For each object, I will examine its SED, ACS image, position on the color magnitude diagram, level of excess, and perhaps other data, and look for revealing connections. Improved models may be fitted to the SEDs to more rigorously characterize the galaxies.

5.2 Summary

This work explored the puzzle of the cause of FIR excess emission in objects on the red sequence that did not have spectroscopic signs of star formation or AGN. First, the red sequence was defined using the straightforward but effective method of delimiting the RS with box chosen by eye. The spectra for these objects were examined for emission lines. The image for these galaxies in multiple bands were compared to verify the 24μm photometry. Then, the RS galaxies without emission lines were studied using CM diagrams, color images, and SED model fitting. The tentative conclusion of this work is that ongoing star formation may be causing the excess, because the objects are brighter and bluer than the general red sequence, and there are visible patches of young stars near them in the color images. The model fitting suggests that the star formation rate has decayed slower for these galaxies than other RS objects. However, the calculated ages also suggest that the galaxies are older. If star formation is the cause, it must be established why emission lines were not observed. Much work remains to reach a definitive conclusion.

References

[1] Strateva, I. et al. 2001, ApJ, 122, 1861

[2] Schneider, P. *Extragalactic Astronomy and Cosmology.* 2006, Berlin, Springer

[3] Bell, E. et al. 2004, ApJ, 600, L11

[4] http://www.ucolick.org/~simard/phd/root/node21.html

[5] Temi, P. Brighenti, F., & Matthews, W. 2007, ApJ, 660, 1215

[6] Davis et al. 2003, SPIE, 4834, 161

[7] Davis et al. 2007, ApJ, 660, L1

[8] http://aegis.ucolick.org/

[9] http://nedwww.ipac.caltech.edu/help/cosmology_calc.html

[10] Ribas, I. et al. 2005, ApJ, 635, L37

[11] http://en.wikipedia.org/wiki/H-alpha

[12] Lorente, R. et. al. AKARI IRC Data User Manual Ver. 1.4 2008

[13] http://en.wikipedia.org/wiki/Point_spread_function

[14] Maraston, C. 2005, MNRAS, 362, 799

[15] Gumley, L. *Practical IDL Programming.* 2002, San Diego, Academic Press